



TAMPEREEN TEKNILLINEN YLIOPISTO
TAMPERE UNIVERSITY OF TECHNOLOGY

ASKO RANTANEN
DESIGN OF A LOW LOSS AND COST-EFFICIENT CHOKE FOR A
GENERAL PURPOSE FREQUENCY CONVERTER

Master thesis

Examiners: Assist. prof. Paavo Rasilo
and Assist. prof. Tuomas Messo
Examiners and topic approved
on 31st of May 2017

ABSTRACT

ASKO RANTANEN: Design of a low loss and cost-efficient choke for a general purpose frequency converter

Tampere University of Technology

Master of Science Thesis, 69 pages, 2 Appendix pages

September 2017

Master's Degree Programme in Electrical Engineering

Major: Power electronics

Examiners: Assistant Prof. Paavo Rasilo, Assistant Prof. Tuomas Messo

Keywords: harmonic distortion, inductor design, choke design, high efficiency, low loss, optimization

Frequency converters are used to operate machines at speeds that are optimal for the process, thus allowing a high efficiency. Frequency converters help save energy but by doing so they also pollute the grid and cause disturbances. These disturbances can be seen in the grid current waveform as harmonic components. The most common way to mitigate harmonic current is to add inductance to the input of the converter by using a choke.

In order to obtain a high efficiency for a choke, the design needs to be optimized. High efficiency needs to be obtained without increasing the size and cost of the choke. In DC and low frequency applications, most of the power losses occur in the windings of the inductor. Optimization process should be targeted to total wire DC-resistance. Small number of turns and large cross-sectional area are needed to achieve the goal.

Different core shapes and winding methods can be used to achieve the best result. Several design constraint drive the design process. In high power applications high saturation current is usually needed. This means that laminated magnetic steel core is usually used due to the material's high saturation flux density.

Three different designs and prototypes are introduced in this thesis. All of the designs utilize different winding methods and core shapes. Matlab is used to optimize the designs and Maxwell is used for magnetic modelling. Inductance, resistance and thermal measurements are carried out on the new designs and reference chokes. Comparison is performed on properties and manufacturability of different solutions. Further development is suggested on the most promising designs.

TIIVISTELMÄ

ASKO RANTANEN: Pienihäviöisen ja kustannustehokkaan kuristimen suunnittelu yleiskäyttö taajuusmuuttajaan.

Tampereen teknillinen yliopisto

Diplomityö, 69 sivua, 2 liitesivua

Syyskuu 2017

Sähkötekniikan diplomi-insinöörin tutkinto-ohjelma

Pääaine: Tehoelektroniikka

Tarkastajat: Assistant Prof. Paavo Rasilo, Assistant Prof. Tuomas Messo

Avainsanat: harmoninen vääristymä, käämisuunnittelu, kuristinsuunnittelu, pienihäviöinen, kustannustehokas, optimointi

Taajuusmuuttajia käytetään esimerkiksi ohjaamaan sähkömoottoreilla toimivia prosesseja. Moottori saadaan pyörimään prosessin kannalta optimaalisella nopeudella, jolloin hyötysuhde kasvaa. Samaan aikaan taajuusmuuttajat tuottavat verkkoon häiriöitä. Nämä häiriöt näkyvät verkkovirrassa harmonisina komponentteina. Induktanssin lisääminen taajuusmuuttajan tulopuolelle kuristimen avulla on yleisin tapa vähentää harmonisia virtoja.

Kuristimen suunnittelu on monivaiheinen prosessi. Suunnittelun lähtökohtana ovat kuristimelle asetetut vaatimukset kuten induktanssi, saturaatiovirta ja sallitut häviöt. Tavoitteiden on oltava selkeät, sillä suunnittelussa joudutaan tekemään kompromisseja eri ominaisuuksien kesken. Pienten tehohäviöiden saavuttamiseksi kuristinsuunnitelma on optimoitava. DC-käytöissä ja pienillä AC-taajuuksilla suurin osa häviöistä syntyy kuristimen käämeissä. Optimoinnin kohteena on tästä syystä käämin DC-resistanssi. Pieni resistanssi voidaan saavuttaa pienellä kierrosmäärällä ja suurella johtimen poikkipinta-alalla.

Kuristimen suunnittelussa käytetään erilaisia käämintämenetelmiä sekä sydänrakenteita. Kuristimelta vaadittujen ominaisuuksien lisäksi suunnittelulle on muitakin rajoitteita kuten paino, tilavaraus ja sallittu lämpeneminen. Suuritehoisissa käytöissä kuristimen saturaatiovirta on yleensä määräävä tekijä, jonka perusteella suunnittelu aloitetaan. Sydänmateriaalina käytetään useasti magneettista terästä, joka sietää suuria magneettivuontiheyksiä saturoitumatta.

Työssä suunnitellaan ja valmistetaan kolme kuristinprototyyppiä, joissa kaikissa käytetään erilasta käämintämenetelmää ja sydänrakennetta. Kuristinsuunnitelmien optimointi suoritetaan Matlab-koodilla. Prototyyppikuristimien magneettiset mallit luodaan Maxwell-ohjelmalla. Prototyyppikuristimien induktanssi, resistanssi ja lämpiäminen mitataan. Mittaustuloksia ja prototyyppien valmistettavuutta verrataan referenssikuristimeen. Lisätutkimusta suositellaan kaikkein lupaavimmalle vaihtoehdolle.

PREFACE

This thesis was written in co-operation with ABB during the spring and summer of 2017. I want to thank Jussi Suortti, Jukka-Pekka Kittilä, Jari Mäkilä, Juha Mikkola and Jarno Alahuhtala for guidance, mentoring and presenting ideas for the thesis. In addition I want to thank Vesa Palojoki for helping with mechanical modelling and the ordering process of the prototypes.

I also want to thank Ville Kourusuo from Trafotek for technical support during the design process and prototype manufacturing. Assistant professors Paavo Rasilo and Tuomas Messo offered excellent guidance and feedback during the writing process.

I want to show gratitude to my wife Emmi for supporting me during my studies. Quitting my previous job and starting to study again was not an easy decision. Your encouragement kept me going forward and gave me motivation to finish my studies well ahead of schedule.

Helsinki, 22.9.2017

Asko Rantanen

CONTENTS

1.	INTRODUCTION	1
2.	HARMONIC DISTORTION CAUSED BY FREQUENCY CONVERTERS	4
	2.1 Frequency converters	4
	2.2 Non-sinusoidal waveforms and harmonic distortion	5
	2.3 Standards on harmonic emissions	9
	2.4 Mitigation of harmonic content.....	12
	2.5 Difference between an AC-choke and a DC-choke	14
	2.6 Conducting EMI.....	15
3.	OPERATION AND DESIGN OF CHOKES.....	17
	3.1 Operation of a choke	17
	3.1.1 Electromagnetic principle	17
	3.1.2 Magnetic circuit and reluctance	20
	3.1.3 Inductance	24
	3.2 Power losses in a choke.....	25
	3.2.1 Winding losses	25
	3.2.2 Iron losses	27
	3.3 Design of magnetic components	28
	3.3.1 Design constraints	28
	3.3.2 Calculating inductance and saturation current	29
	3.3.3 Thermal behaviour	30
	3.3.4 IP-class	33
	3.4 Core design.....	34
	3.4.1 Core materials	34
	3.4.2 Shape of the core.....	36
	3.5 Winding design	37
	3.5.1 Winding materials	37
	3.5.2 Winding methods	38
4.	DESIGN OF A NEW DC-CHOKE	41
	4.1 Baseline and objectives for the design	41
	4.1.1 Objective of the design	41
	4.1.2 Reference chokes	42
	4.2 Design process.....	44
	4.2.1 Design flow	45
	4.2.2 Optimization with Matlab	46
5.	NEW DESIGNS AND PROTOTYPES.....	50
	5.1 Intorduction of new designs and prototypes	50
	5.1.1 Design A	50
	5.1.2 Design B.....	53
	5.1.3 Design C.....	56
	5.2 Test results.....	57

5.2.1	Inductance measurement.....	57
5.2.2	Resistance measurement	58
5.2.3	Thermal behaviour	59
5.3	Cost estimate and manufacturability	62
6.	CONCLUSIONS.....	64
	REFERENCES.....	67

APPENDIX A: AN EXAMPLE OF THE MATLAB SCRIPT USED FOR OPTIMIZATION

SYMBOLS AND ABBREVIATIONS

ASD	Adjustable speed drive
AFE	Active front end
EMC	Electromagnetic compatibility
EMI	Electromagnetic interference
GO	Grain oriented
IEEE	Institute of Electrical and Electronics Engineers
IEC	International Electrotechnical Commission
IGBT	Insulated gate bipolar transistor
IP	Ingress protection
MPL	Mean path length
NO	Non-oriented
PWM	Pulse width modulation
TDD	Total demand distortion
THD	Total harmonic distortion
PF	Power factor
PPC	Point of common coupling
PWHD	Partially weighed harmonic distortion
RMS	Root mean square
SMC	Soft magnetic composite
VSD	Variable speed drive
α	Steinmetz's equation parameter for frequency
β	Steinmetz's equation parameter for flux density
ϵ	Emissivity of a material
δ	Skin depth
λ	Conductivity of a material
μ_{core}	Permeability of the core material
μ_0	Permeability of free space
μ_{eff}	Effective permeability
μ_r	Relative permeability
\mathfrak{R}	Reluctance
$\mathfrak{R}_{\text{gap}}$	Reluctance of the air gap
$\mathfrak{R}_{\text{core}}$	Reluctance of the core
ρ	Resistivity
σ	Stefan-Boltzmann constant
τ	Time constant
φ	Phase angle between voltage and current
Ψ	Flux linkage
ω	Angular frequency
A	Cross-sectional area
A_{core}	Cross-sectional area of the core
A_{gap}	Cross-sectional area of the air gap
A_t	Effective heat dissipating surface area
A_w	Cross-sectional area of the conductor
B	Magnetic field density

B_{\max}	Maximum magnetic field density
B_{sat}	Saturation magnetic field density
C_m	Thermal coefficient of resistance
E	Electric field strength
e	Electromagnetic force
F	Magnetomotive force
F_{FF}	Fringing flux factor
f	Frequency
H	Magnetic field strength
h_c	Heat transfer coefficient
i_L	Inductor current
I_L	Maximum load current
I_{peak}	Peak current
I_{RMS}	RMS current
I_{sat}	Saturation current
I_{SC}	Maximum short circuit current
J	Current density
L	Inductance
k	Steinmetz's equation coefficient
l_{gap}	Length of the air gap in a magnetic circuit
l_{core}	Length of the core in a magnetic circuit
l_h	Height of a thermal object
l_c	Total distance passed by the cooling medium
l_w	Length of the conductor
N	Number of turns
P	Active power
P_{AC}	AC power loss
P_{DC}	DC power loss
P_E	Eddy current power loss
P_S	Skin effect power loss
PF_{disp}	Displacement power factor
PF_{dist}	Distortion power factor
P_m	Permeance
R	Resistance
R_T	Resistance at temperature T
R_{th}	Thermal resistance
R_{cd}	Thermal resistance of conduction
R_c	Thermal resistance of convection
R_r	Thermal resistance of radiation
R_{sce}	Short circuit ratio
Q	Reactive power
Q_v	Core loss per volume
S	Apparent power
V	Volume
v	Velocity of cooling medium
W	Energy
W_{gap}	Energy stored in the air gap
W_{field}	Field energy
ΔT	Change in temperature

T	Temperature
T_0	Initial temperature
u_L	Inductor voltage

1. INTRODUCTION

A substantial amount of the electricity produced in the world is consumed by different kinds of electrical motors or machines. Frequency converters allow these machines to be operated at speeds that are optimal for the process, thus allowing high efficiency. Frequency converters are really common and their development has been rapid during the last decades. Frequency converters used to control electric motors are commonly called adjustable speed drives (ASDs) or variable speed drives (VSDs).

The industry is constantly looking for more ways to save energy and increase efficiency. It is no longer enough that the VSD saves energy and lowers the power losses of the process controlled by the electric motor. The power losses of the drive itself must also be minimal. Research is leaning toward higher power density and efficiency [1]. The drawback is that higher power density and efficiency usually spells out higher cost.

There are a lot of variables that affect the decision of purchasing a VSD. The customer's initial demand is the ability to control the process more accurately and save energy. Even though the payback time of a frequency converter is relatively short compared to many other investments, the price of the converter plays a big role in making the purchase decision. Other factors like weight, volume and failure rate are also considered.

There are a lot of manufacturers on the field and competition is tough. It has proven hard to increase the efficiency of the controlled motor or to reduce the cost significantly compared to competitors. This has invoked an interest in the power losses of the VSD itself as a means of differentiating the product from the competition.

The power losses of the converter are usually relatively small compared to those of the controlled motor, but when it comes down to making an investment decision, smallest of details might make the difference. Let's say there are two VSDs with the same specifications and price tags. If one or the other can advertise itself to consume less energy than the competitor it might be the factor that will seal the deal.

Frequency converters help save energy but by doing so they also pollute the grid and cause disturbances. Most general purpose VSDs are equipped with a diode bridge rectifier. This causes the converter to draw intermittent current from the grid and it can be seen as harmonic current components in the grid current waveform. These harmonics can increase line losses, distort the voltage waveform, heat transformers, damage equipment connected to the same network and waste energy [2]. That is just the opposite of what the converter is supposed to do. Hence grid-connected converters are expected to meet electromagnetic compatibility (EMC) standards set out by organizations like the International

Electrotechnical Commission (IEC) and the Institute of Electrical and Electronics Engineers (IEEE).

There are different methods for mitigating these harmonics, but a choke is by far the most common solution. Adding inductance smooths the current waveform and thus cuts down the harmonic content. The DC capacitor will be charged for a longer time. This means that the current pulse is wider and the peak of the pulse is lower. The choke can be placed either on the AC-line side or the DC-link side of the rectifier.

Chokes are fairly simple components, but they are usually big, bulky, heavy and expensive. Chokes can be bought off the shelf but they are rarely suited for a specific application. Careful and thorough optimization should be done for individual applications in order to guarantee high efficiency.

The purpose of this thesis is to design a new high efficiency and low cost DC-link choke for a frequency converter. This wall mount converter is a part of ABB's low power drives product line. The baseline for the new design is an existing DC-choke. An existing DC-choke and an AC-choke variant are used as reference for measurements. Power loss measurements have revealed that the input side power losses of the converter were higher than had been initially anticipated. The goal is to achieve lower power losses using the same space and at the same cost.

Transformers and chokes have been built in the same manner for the past century. Improvement can be achieved with unconventional choice of materials and winding techniques. With high current and low frequency, winding losses play a major role in total power loss. The obvious target for improvement is the power losses of the windings. Chokes are usually wound with copper windings due to its high conductivity, but copper is rather expensive. The same properties can be achieved by using aluminium which is a lot cheaper. On the other hand copper has lower resistance so a larger amount of aluminium is needed to keep the losses down. Different winding techniques can be used to fit the same amount of wire to a smaller window. However these winding techniques may be harder to execute.

This thesis will begin with an introduction to the design of magnetic components. Overview of harmonic distortion and mitigation is given in Section 2. Standards that govern harmonic emission levels are also introduced in this chapter. Necessary concepts and equations needed in the design process of inductive components are presented in Section 3. Different forms of power losses that occur in chokes are also presented. Using this theory a new design is implemented in Section 4. A series of measurements are done on existing chokes in order to obtain the baseline for the new choke design. A Matlab-script is used to optimize the new choke designs. Different options are evaluated and prototypes of the most appealing designs will be ordered. The operation of the prototypes will be discussed in Section 5. The same measurements are carried out for the prototypes and

their operation will be compared to the reference DC-choke. Inductance, power losses and thermal behaviour are the main points of interest. Lastly the cost and manufacturability of the new choke designs are evaluated and compared to the reference chokes. The final section will present the results and conclusions of the thesis.

2. HARMONIC DISTORTION CAUSED BY FREQUENCY CONVERTERS

This section presents an introduction to frequency converters and harmonic currents. An overview of international standards for harmonic emission limits is given and the most common ways to mitigate harmonic currents are also presented.

2.1 FREQUENCY CONVERTERS

Frequency converters are used to modify the amplitude and frequency of the grid voltage to desired levels. These converters are usually used together with electric motors or generators. The energy taken from or fed to the grid can be regulated closely. Without frequency converters electric machines would operate at the speed determined by the grid frequency and generators could feed electricity to the grid only if they were operating at the grid frequency. Changes in speed would have to be made mechanically using valves or gears depending on the application. These mechanical parts can be expensive and are usually suited for particular applications only. They are not interchangeable between different setups. Using mechanical means to control the process is not efficient. The system output is running at the desired speed, but the motor driving the system is still running at full speed and consuming more energy than necessary. Frequency converters allow a much higher efficiency by controlling the speed of the electric motor driving the process.

Multiple topologies for three phase frequency converters have been developed, but the most common topology utilises a six step diode bridge rectifier at the input, a DC-link capacitor and an active inverter bridge at the output [3]. A common 6-step topology is presented in Figure 1.

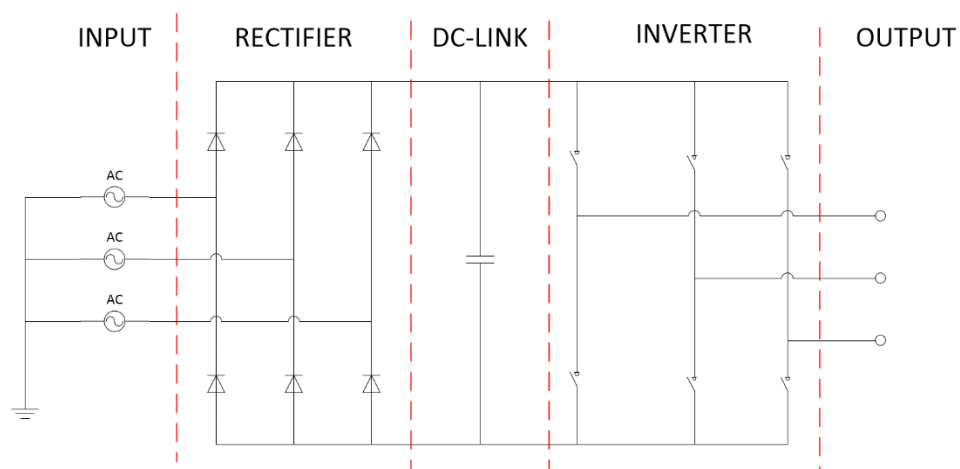


Figure 1 Power stage of a frequency converter with a common 6-step diode bridge topology. The frequency converter consists of a rectifier, DC-link and an inverter.

Alternating current from the grid is rectified using the 6-step diode bridge. The states of the diodes will change according to the sinusoidal voltage of the supply. Only one of the diodes on both the high and low side are conducting at the same time. The voltage at the output of the rectifier is the same as the voltage between the lines of the conducting diodes. In the case of the 6-step rectifier, the output voltage has six pulses during one cycle of the supplying voltage. The resulting voltage at the output of the rectifier is pulsating DC-voltage. This pulsating voltage is filtered out with a big capacitor in the DC-link which provides a steady DC-voltage to an inverter bridge consisting of insulated gate bipolar transistors (IGBTs). The switches are turned on and off in such a way that the output voltage resembles a sine wave. A pulse width modulation (PWM) scheme can be used to control the output voltage and frequency. The maximum output voltage is dependent on the voltage at the DC link. It is important to achieve a low voltage drop at the input stage of the converter to get the best performance possible. The waveforms of input voltage and input current of one phase are presented in Figure 2.

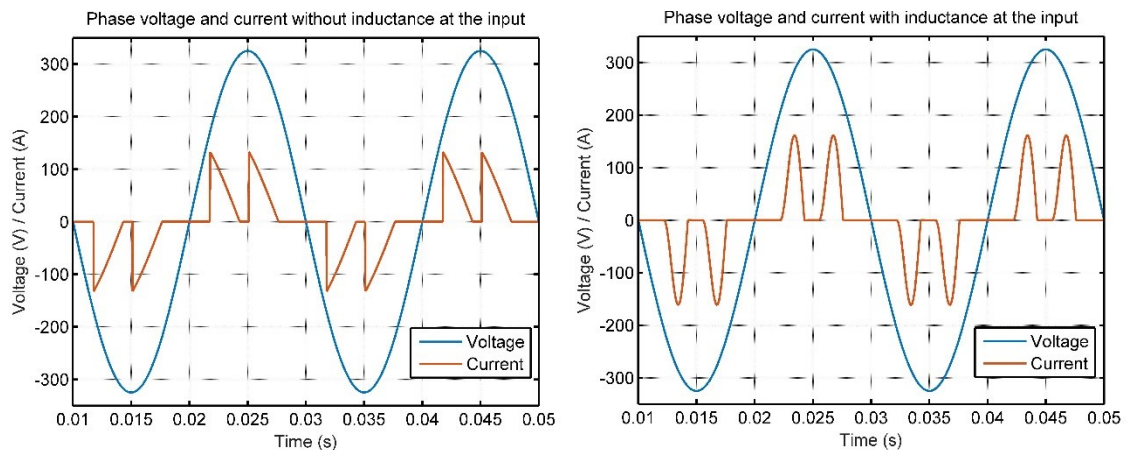


Figure 2 Phase voltage and phase current of a 6-step converter. Current spikes can be seen at points where the line-to-line voltage is greater than the DC-link voltage.

It can be seen from the figure that the input current of the frequency converter is intermittent and far from sinusoidal. The load is said to be non-linear. The chart on the left represents an ideal situation where the grid voltage is purely sinusoidal and stray inductance from the supplying network is neglected. In reality there is stray inductance in the grid which opposes the change in current, causing a sloping increase of the current instead of instantaneous rise. Adding further inductance to the circuit can be used to shape the waveform and reduce harmonic distortion. This is shown in the chart on the right.

2.2 NON-SINUSOIDAL WAVEFORMS AND HARMONIC DISTORTION

A linear load takes current that is in proportion to voltage. The amplitude or phase of the current might differ but the overall shape of the waveform is identical to the voltage waveform. Apparent power S consists of active power P and reactive power Q . Real

power results from current that is in phase with voltage. Reactive power results from current that is out of phase with voltage. Reactive power is pulsating between supply and load but it is not contributing to the work being done and it is not desired. In the case of linear loads power factor describes the relation between active power and reactive power. A high power factor is desired in high efficiency operations. For sinusoidal waveforms it can be calculated with

$$PF = \frac{P}{S} = \frac{VI \cos \varphi}{VI} = \cos \varphi , \quad (1)$$

where V is voltage, I is current and φ is the phase difference between them.

Harmonic distortion is caused by non-linear loads. A non-linear load's impedance changes under alternating voltage. This causes non-uniform voltage and current waveforms. If a sinusoidal voltage is applied to a non-linear load, sinusoidal current is not drawn, as was shown in Figure 2. Diode rectifiers that are usually used in frequency converters are highly non-linear loads. Diodes are either in a conducting or non-conducting state depending on the voltage applied over them. This results in a non-sinusoidal pulsating current.

Non-sinusoidal waveforms can be broken into the fundamental frequency and harmonic components according to Fourier analysis [4]. Harmonic components are sinusoidal waveforms which have frequencies that are multiples of the fundamental frequency. If utility input voltage is approximated to be purely sinusoidal at the fundamental frequency, input current waveform can be presented by the sum of the fundamental frequency and the harmonic components by

$$i_{ac}(t) = i_1(t) + \sum_{h=2}^{\infty} i_h(t), \quad (2)$$

where $i_1(t)$ is the fundamental component of current and $i_h(t)$ is the harmonic component. Sum of the harmonic current components is called distortion current. As can be seen from (2), harmonic content is added on top of the fundamental frequency current. Harmonic components have different frequency than the supplying voltage so they do not contribute to active power. However they do increase the RMS value of the current which in turn increases power losses. Average current delivered to the converter is the same, but due to non-sinusoidal waveform of the current, the RMS value of the current is higher.

In the case of non-sinusoidal waveforms power factor is the product of displacement power factor and distortion power factor. Definitions used for describing power factor of non-sinusoidal waveforms are presented in [5]. Displacement power factor is caused by the phase difference between the fundamental current and voltage, while distortion power factor is due to harmonic content in the waveform. Power factor for non-sinusoidal waveforms can be calculated with

$$PF_{\text{total}} = PF_{\text{dist}} * PF_{\text{disp}} = \frac{I_1}{I_{\text{tot}}} \cos \varphi, \quad (3)$$

where $I_{\text{tot}} = \sqrt{I_{\text{active}}^2 + I_{\text{reactive}}^2 + I_{\text{harmonic}}^2}$. Composition of total current is presented in Figure 3. It can be seen from (3) that in addition to the phase angle, total power factor is also dependent on the amount of distortion current in the system. Power factor decreases as the amount of distortion current increases.

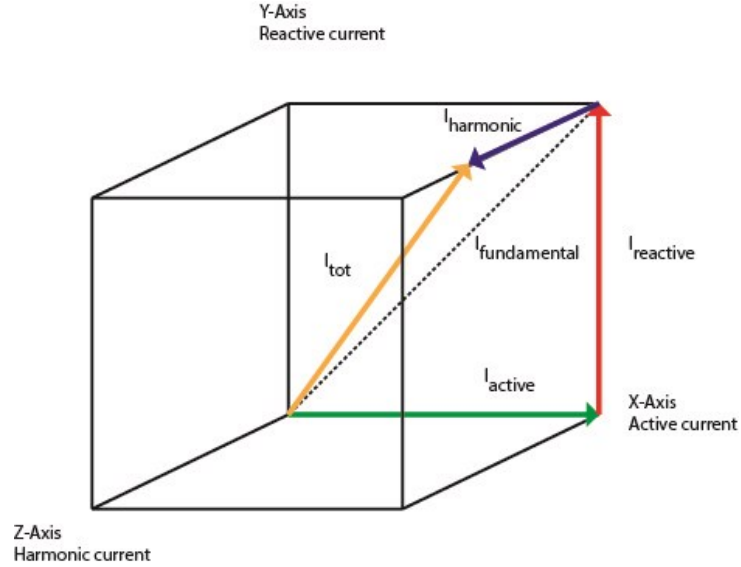


Figure 3 Vector representation of total current including active, reactive and harmonic current. Active current is in the direction of the X-axis, reactive current in the direction of Y-axis and harmonic current is in the direction of Z-axis.

Different rectifier topologies produce different kind of harmonics. In ideal rectifiers the characteristic harmonics depend on the number of pulses in a cycle [4]. The order of harmonic frequencies associated with the common 6-step rectifiers can be found using

$$h = 6k \pm 1, \quad k = 1, 2, 3 \dots \quad (4)$$

The magnitude of these harmonic currents can be obtained from

$$I_h = \frac{I_1}{h}. \quad (5)$$

In order to demonstrate harmonics, Matlab Simulink is used to simulate the 6-step diode rectifier of the converter that was presented in Figure 2. Ideal components are used and stray inductance of the grid is neglected. Fast Fourier transform is performed on the phase current. Harmonic content caused by the rectifier is shown in Figure 4. The fundamental frequency is seen at 50 Hz and harmonic content can be seen at multiples of the fundamental frequency according to (4) and (5).

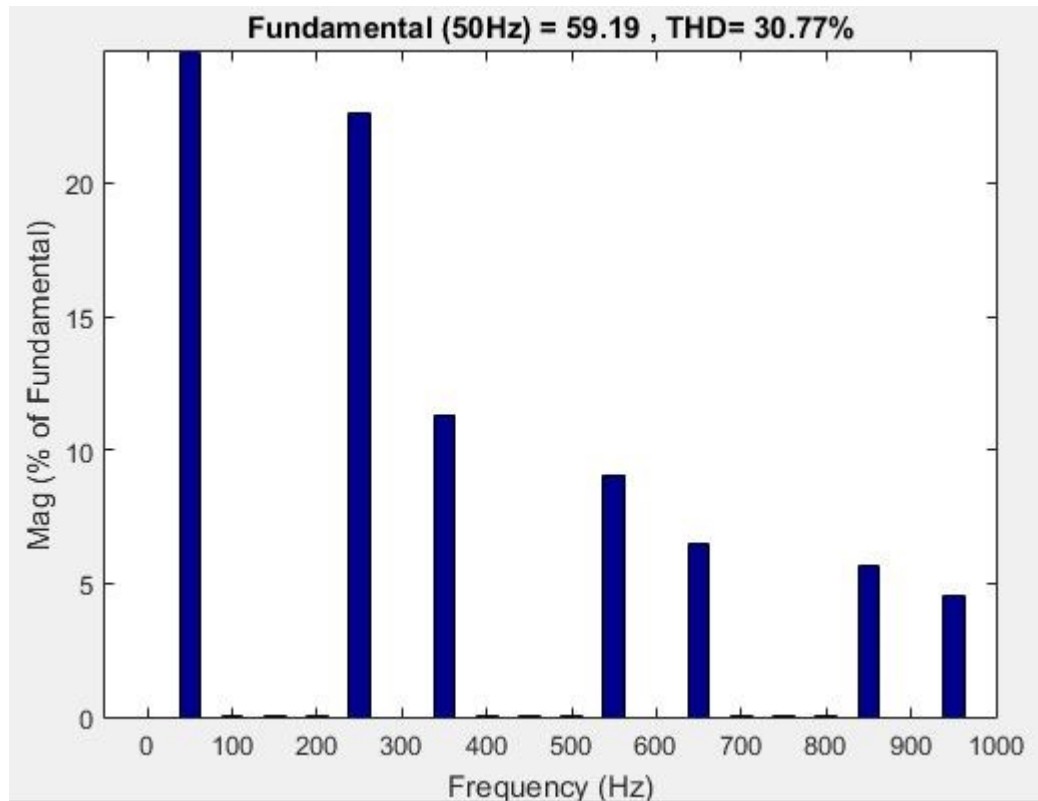


Figure 4 Harmonic content of the input current of a 6-step rectifier. Harmonic components can be seen at multiples of the fundamental frequency. Magnitude of the harmonic components is presented as a percentage of the fundamental frequency.

The total harmonic content can be evaluated by an index called total harmonic distortion (THD). This index is a ratio of the RMS value of total harmonic current and the RMS value of fundamental current. THD of the line current can be calculated using

$$THD = \frac{\sqrt{I_{RMS}^2 - I_1^2}}{I_1}, \quad (6)$$

THD can be used to evaluate the effect of harmonics and compare different solutions. International standards specify levels of allowed THD. Limits are also placed on individual harmonics. The effect of higher order harmonics can be evaluated by using partially weighed harmonic distortion (PWHHD). This eliminates the need for individual limits for every single higher order harmonic. PWHHD from the 14th harmonic up to the 40th can be calculated with

$$PWHHD = \sqrt{\sum_{h=14}^{40} h \left(\frac{I_h}{I_1}\right)^2}. \quad (7)$$

The diode rectifier is a major contributor to harmonics but it is not the only section creating harmonic distortion. Harmonic distortion is also generated for example by dead time effect in the switches at the output of the converter [6].

2.3 STANDARDS ON HARMONIC EMISSIONS

Several international standards give limits for harmonic emissions and offer suggestions on how to achieve these limits. IEEE standard 519-2014 presents recommended practice and requirements for harmonic control in power systems. Harmonic limits for both voltage and current are recommended in the standard. The standard does not set limits for individual equipment. Instead the limits are given for individual users.

Harmonic distortion is observed at a point where the system connects to the utility and other users. This point is called the point of common contact (PCC). For industrial uses this point is usually at the high side of the transformer supplying the plant. For commercial users that share the supplying transformer, the PCC is usually at the low side of the supplying transformer where the user connects to the rest of the users.

IEEE standard aims for a shared responsibility and harmonic distortion limits are set for both the utility and end-users. The utility provider is responsible for the amount of voltage distortion in the line. The inherent distortion in the power system is required to be small. Users are responsible for the current harmonics injected in to the grid. Current emissions must be small enough not to cause voltage distortion above the limits. Voltage distortion limits for different size systems are presented in Table 1.

Table 1 IEEE Standard 519-2000 harmonic voltage limits [7].

Bus voltage V at PCC	Individual harmonic (%)	Total harmonic distortion THD (%)
$V \leq 1.0$ kV	5.0	8.0
1 kV $< V \leq 69$ kV	3.0	5.0
69 kV $< V \leq 161$ kV	1.5	2.5
161 kV $< V$	1.0	1.5 ^a

^aHigh-voltage systems can have up to 2.0% THD where the cause is an HVDC terminal whose effects will have attenuated at points in the network where future users may be connected.

The utility grid is responsible for maintaining voltage distortion at the limits given in the table. In order for this to be possible, current emission limits are set for the customer. Users are divided into categories based on their maximum demand load current I_L and available short-circuit current I_{SC} . Customers with a large I_{SC}/I_L -ratio make up only a small part of the total demand. Thus more distortion is allowed for these users. The limits

get stricter as the ratio decreases. The allowed harmonic current emission levels are presented in the form of total demand distortion (TDD) according to

$$TDD = \frac{\sqrt{\sum_{h=2}^{50} I_h^2}}{I_L} \quad (8)$$

RMS value of the total harmonic current is compared to the RMS value of maximum demand load current of the user. Harmonic currents are calculated up to the 50th harmonic. Limits are also set for individual harmonics. These limits are presented in Table 2.

Table 2 IEEE Standard 519-2000 harmonic current limits [7].

Maximum harmonic current distortion in percent of I_L						
Individual harmonic order (odd harmonics)^{a, b}						
I_{sc}/I_L	$3 \leq h < 11$	$11 \leq h < 17$	$17 \leq h < 23$	$23 \leq h < 35$	$35 \leq h \leq 50$	TDD
$< 20^c$	4.0	2.0	1.5	0.6	0.3	5.0
$20 < 50$	7.0	3.5	2.5	1.0	0.5	8.0
$50 < 100$	10.0	4.5	4.0	1.5	0.7	12.0
$100 < 1000$	12.0	5.5	5.0	2.0	1.0	15.0
> 1000	15.0	7.0	6.0	2.5	1.4	20.0

^aEven harmonics are limited to 25% of the odd harmonic limits above.

^bCurrent distortions that result in a dc offset, e.g., half-wave converters, are not allowed.

^cAll power generation equipment is limited to these values of current distortion, regardless of actual I_{sc}/I_L .

where

I_{sc} = maximum short-circuit current at PCC

I_L = maximum demand load current (fundamental frequency component)
at the PCC under normal load operating conditions

IEEE standard is practical to implement in facilities but it is not that helpful in the design process of an individual VSD. Short circuit current of the PCC and the total current demand of the user are usually not known at the time of design.

IEC standards have a different approach and limits for individual equipment are given. IEC 61000 standard collection deals with electromagnetic compatibility. The collection consists of terminology, general information, installation guidelines and techniques for testing and measurement. Part 3 of the collection is dedicated to emission limits. IEC has also published 61800 standard that is dedicated to VSDs. This standard lists all important standards that need to be taken into account when dealing with VSDs. The most important standards are given in Table 3.

Table 3 IEC standards on emission limits [8].

Standard	Description
IEC 61000-3-2	Limits for harmonic current emissions (equipment input current ≤ 16 A per phase)
IEC 61000-3-4	Limitation of emission of harmonic currents in low-voltage power supply systems for equipment with rated current greater than 16 A
IEC 61000-3-12	Limits for harmonic currents produced by equipment connected to public low-voltage systems with input current > 16 A and ≤ 75 A per phase
IEC 61800	Adjustable speed electrical power drive systems - Part 3: EMC requirements and specific test methods

It can be seen from the table that there are different standards for equipment with different nominal currents. The allowed levels of THD for equipment with nominal current between 16 and 75 A are presented in Table 4. Harmonic limits are set based on the short-circuit ratio R_{sce} which is a ratio between the short-circuit power of the system and the apparent power of the equipment. A larger THD is allowed for equipment with high short-circuit ratios.

Table 4 IEC 61000-3-4 current emission limits for balanced three phase equipment [9].

Minimal R_{sce}	Admissible harmonic current distortion factors		Admissible individual harmonic current I_n/I_1^*			
	%		%			
	<i>THD</i>	<i>PWHD</i>	I_5	I_7	I_{11}	I_{13}
66	16	25	14	11	10	8
120	18	29	16	12	11	8
175	25	33	20	14	12	8
250	35	39	30	18	13	8
350	48	46	40	25	15	10
450	58	51	50	35	20	15
600	70	57	60	40	25	18
NOTE 1 – The relative value of even harmonics shall not exceed $16/n$ %.						
NOTE 2 – Linear interpolation between successive R_{sce} values is permitted.						
* I_1 = rated fundamental current; I_n = harmonic current component.						

However there is no standard for harmonic emission limits for equipment with a higher nominal current than 75 A. In these cases the supply authority may accept the connection of the equipment on basis of the agreed active power of the user's installation [9]. Local requirements of the power supply authority apply in this case. Manufacturer has to provide information on individual measured harmonics and the values for THD and PWHD. These values may be presented by calculations, simulations or measurements.

The harmonics are typically counted up to the 40th harmonic in IEC standards. THD is usually observed in current but it can be presented for voltage as well. Voltage distortion appears whenever harmonic current passes through the impedance of the supplying network. The relationship between harmonic current distortion and harmonic voltage distortion can be inductive, capacitive or resistive and not fully linear.

2.4 MITIGATION OF HARMONIC CONTENT

There are multiple ways to mitigate harmonic distortion, but the most common way is to add inductance to the input of the converter [10]. An AC-choke is placed in front of the converter before the rectifier. A single individual choke can be placed on all phase lines, but it is more common to use a three phase choke where all phase lines share a common core. This reduces cost and saves space.

A DC-choke is placed after the rectifier on the positive and negative DC-voltage bars. Differences between these two basic approaches are presented in Section 2.5. Adding inductance cuts down harmonics and improves power factor. Additional power losses occur in the chokes but they are necessary to improve the performance of the drive.

Different ways to mitigate harmonics besides using chokes are presented in [10]. Filters or harmonic traps can be used to suppress the harmonic frequency. Filtering can be done with a passive or an active filter. In the case of a 6-pulse rectifier 5th and 7th harmonics are the strongest so the passive filter should be tuned close to those frequencies. These filters need to be carefully planned in order to avoid system resonance. Active filters supply the harmonic current that the non-linear load needs and corrects the power factor of the drive. Harmonic current is not drawn from the utility. Reactive power flows back and forth between the filter and the drive. Line current is not affected by the harmonics and there is no distortion.

Adding pulses to the rectifier helps to smooth the grid current. A 12-step, 18-step or even 24-step rectifiers are used. These methods improve the grid current waveform significantly. On the downside using these methods requires the use of two transformers. They are more expensive than a regular 6-step rectifier and take up a lot more space. Power losses in the rectifier are increased as well. It is also impossible to retrofit this method to existing VSDs.

The diodes in the rectifier can be replaced with switches. This is called an active front end (AFE). The switches can be controlled in order to draw undistorted sine-shaped current from the grid. Current drawn is basically almost sinusoidal. AFE is an efficient way to reduce harmonics. However it is more expensive than a diode bridge. General comparison of different harmonic mitigation methods is given in [11]. Characteristics of these different solutions are presented in Table 5.

Table 5 Characteristics of different harmonic mitigation solutions [11] .

	AC choke	DC choke	12-pulse VFD	Passive filter	Active filter	Hybrid filter
Current THD(%)	< 40%	< 45%	< 11 %	<12%	3-5%	5-7%
Efficiency	Moderate	Moderate	High	Moderate	High	High
Overall dimension	Small	Small	Large	Large	Large	Large
Complexity	Simple	Simple	Complicated	Moderate	Very complicated	Very complicated
Cost	Low	Low	Expensive	Moderate	Very expensive	Very expensive

It can be seen that chokes are not the best in performance, but they are by far the cheapest option. In mass produced general purpose drives cost is really important. It is also noteworthy that there is no point in reducing the harmonics excessively. If a convenient level can be reached with a cheaper option, it should be used before venturing into the more expensive options.

On top of these methods proper care should be taken in installing the equipment. Part 5 of IEC 61000 standard collection gives guidelines for proper installation of equipment and general ways for harmonic mitigation. These guidelines consist of actions that the user can take in order to meet the emission limits.

It's also worth remembering that THD is a ratio which means that it can be decreased either by lowering the harmonic components or by increasing the fundamental component by adding linear load. The amount of inductance in the feeding grid also affects the amount of harmonic current.

2.5 DIFFERENCE BETWEEN AN AC-CHOKE AND A DC-CHOKE

The main purpose of a choke is to reduce harmonics by adding inductance to the input side of the VSD. Depending on application this inductance can be added either before the rectifier on the AC-line side or after the rectifier to the DC-link side. Both approaches are used in the industry. According to [12] better harmonic mitigation for the same amount of inductance is achieved with an AC-line choke. In order to obtain the same THD reduction a DC-link choke needs to have twice the inductance of the line inductance of the AC-line choke [12]. Placement of line and link choke in a typical VSD topology is presented in Figure 5.

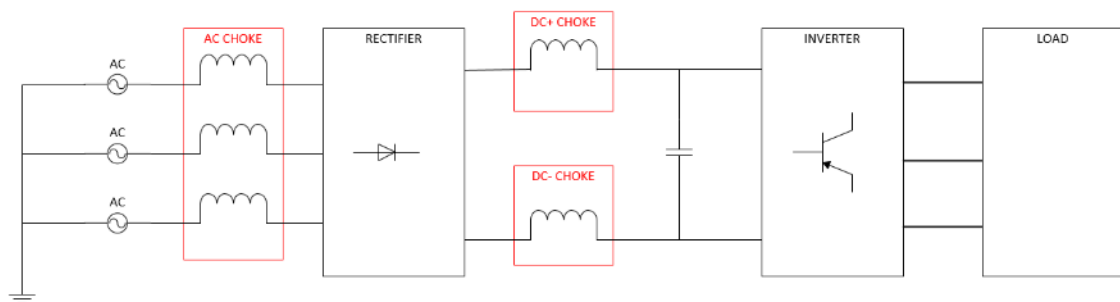


Figure 5 AC- and DC-choke placement in a conventional VSD topology.

AC-choke is a series connected component which is connected so that all of the line frequency current of three phases will pass through it. Increased inductance at the input of the choke creates diode commutation overlap in the rectifier. This increases the voltage drop across the choke and rectifier. The effective voltage in the DC-link is thus lower. Lower DC-voltage means lower voltage at the output of the converter. This can reduce the output power of the converter which is not desirable. DC-chokes are placed after the rectifier so the voltage drop applies only to the ripple, not the overall level of DC voltage. Commutation overlap is also decreased which means that the voltage drop is smaller if DC-chokes are used.

The difference between the voltage drop of AC- and DC-chokes has been studied in [13]. Depending on the case the voltage drop of a DC-choke can be as much as three times smaller than the voltage drop of an AC-choke. On the upside AC-choke protects the circuitry from possible current spikes or voltage surges. In the case of DC-chokes the inductors are placed after the diode bridge, so they don't offer any surge protection to the rectifier. If surge protection is needed it has to be done with separate components like varistors, which increases cost.

As shown in Figure 5, DC-chokes are usually placed in both the positive and negative bus bars of the DC-link. This is done to eliminate EMI problems like common-mode currents. AC-chokes can be manufactured as single phase or three phase chokes. The functionality

is the same in both cases, but the three phase version usually requires less material. Line choke could be made from three separate single phase chokes for each line, but this would require three different cores. The 120 degrees phase difference in line currents allows using a common three legged core for all the phases.

2.6 CONDUCTING EMI

Chokes are mainly used for harmonic mitigation but they can have a big impact on other conducting electromagnetic interference (EMI) issues as well. Main idea of the choke is to increase differential inductance in the circuit, but if common mode inductance can be added to the design it might improve the overall performance of the VSD. Common-mode currents flow in the same direction and form a closed loop through parasitic capacitances to earth. If the choke is only on the positive or negative bus bar, proper common-mode inductance is not achieved. Common-mode voltage causes EMI issues and gives rise to bearing currents. Difference between common-mode and differential mode currents are presented in Figure 6.

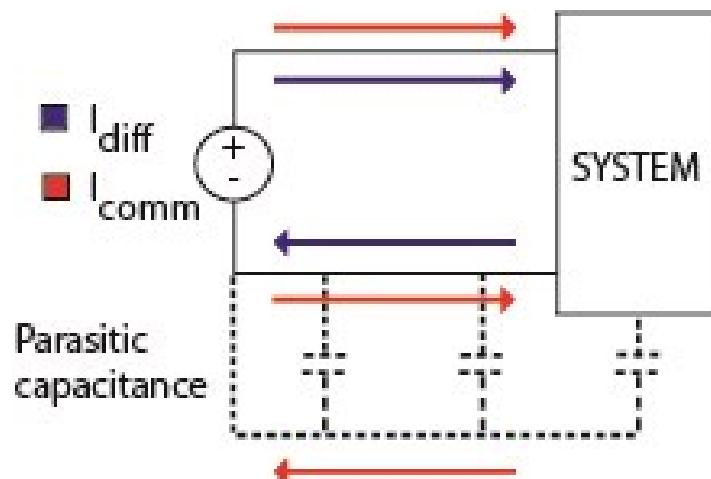


Figure 6 Difference between common-mode and differential mode currents. Common-mode current forms a closed loop outside of the system.

Common DC-choke topology with two separate chokes on both the positive and negative bus bar offers common mode inductance alongside with differential inductance. AC chokes are usually manufactured as three-legged cores that lack common mode inductance. Flux is not created by common mode current because there is no small reluctance return path. Adding an extra leg would allow a return path for common mode flux, but it increases the required size and cost of the choke. This is demonstrated in Figure 7.

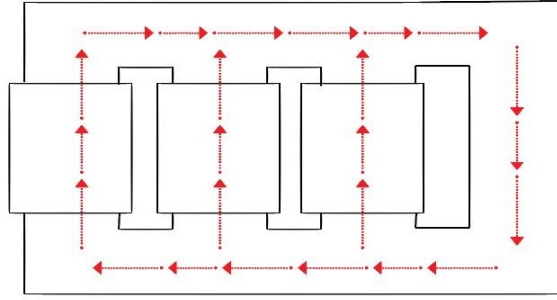


Figure 7 Flux direction in the case of an AC-choke with differential and common-mode inductance. The extra leg allows a low reluctance path for common-mode flux.

It can be seen from Figure 7 that the size of the choke is increased if the extra leg is added. Separate common-mode chokes are used to further suppress common-mode currents.

3. OPERATION AND DESIGN OF CHOKES

This section presents the electromagnetic theory needed in choke design. Different aspects that need to be addressed in the design process are also introduced. These include power losses, thermal behaviour and different core and winding materials. Common design constraints that set boundaries to the design are also discussed.

3.1 OPERATION OF A CHOKE

A choke is an inductor whose primary purpose is to oppose the changes in current. Inductors have a core made of magnetic material and a coil wrapped around it. Operation of electromagnetic components can be described by the Maxwell equations. Especially Faraday's law and Amperé's law are crucial in inductor design. The purpose of a choke is to add inductance to the input of the VSD. A choke needs to have a proper amount of inductance in order to attenuate harmonic currents.

3.1.1 Electromagnetic principle

According to Amperé's law, current in a conductor creates a magnetic field around the conductor that is proportional to the flowing current [14]. The magnetic field is characterized by magnetic field strength H and magnetic field density B . Magnetic field strength and density are measured in amperes per meter [A/m] and teslas [T], respectively.

The direction of the magnetic field is determined by the direction of the current. The right hand rule can be used to point the direction of the magnetic field. If the right thumb is aligned in the same direction with current flow, the direction of the magnetic field will be pointed out by the rest of the fingers. Amperé's law can be presented in integral form using the magnetic field strength by

$$\oint_l \vec{H} \cdot d\vec{l} = \int_S \vec{J} \cdot d\vec{a}, \quad (9)$$

where l is the length of the magnetic path, \vec{J} is the current density vector and a is the surface area that the current is passing through. The left hand side integral represents the magnetomotive force (MMF) and the right hand side integral is the total current passing through the area. If the conductor is wound into a winding, the right hand side integral can be presented with the product of the current flowing in the conductor and the number of turns in the winding. In the case of a uniform magnetic field strength across an element, (9) is reduced to

$$F = Hl = Ni, \quad (10)$$

where F is the MMF, N is the number of turns in the winding and i is the current flowing in the conductor. The unit of MMF is ampere-turn [At]. The MMF causes magnetic flux to flow in the magnetic circuit. Magnetic flux is denoted by Φ and it is measured in webers [Wb]. If the same amount of flux is passing through every turn of the coil, flux linkage Ψ linking these turns can be calculated by

$$\Psi = N\Phi. \quad (11)$$

Faraday's law states that a changing magnetic field induces an electromotive force (EMF) that causes a current in a closed loop [14]. Faraday's law can be presented in integral form

$$\oint_1 \bar{E} \cdot d\bar{l} = -\frac{d}{dt} \oint_S \bar{B} \cdot \bar{n} da, \quad (12)$$

where E is the electric field strength, B is the magnetic field density and \bar{n} is normal vector of the surface. If uniform and perpendicular flux density is approximated, the equation can be presented with

$$e = -\frac{d\Psi}{dt} = -N \frac{d\Phi}{dt}, \quad (13)$$

where e is the EMF and Ψ is the flux linkage. As can be seen from (13), the EMF opposes the change in flux linkage. A magnetic circuit representing these equations is presented in Figure 8.

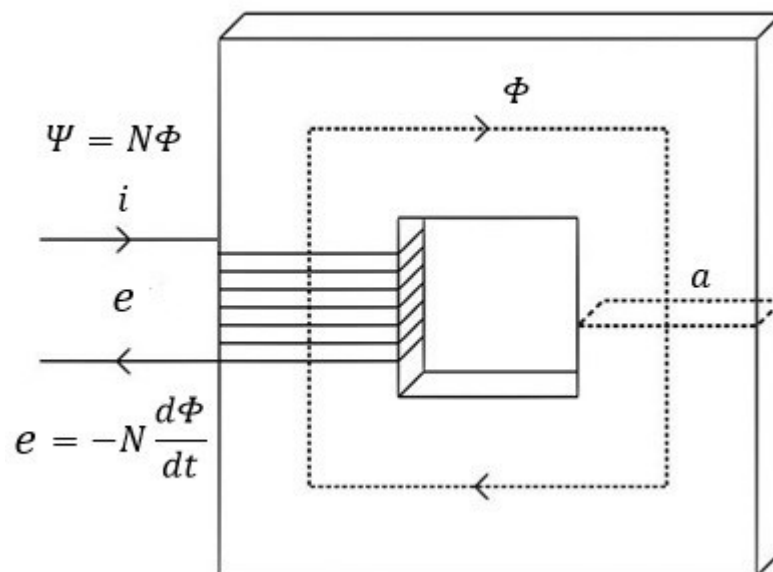


Figure 8 Magnetic core with N turns of wire in a coil. Magnetic flux flows in the core with uniform distribution. Voltage over the coil is equal to the EMF.

Gauss's law for magnetic field states that the total magnetic flux through a closed surface is zero [14]. This means that flux lines are continuous and the same amount of flux must enter and exit the surface. Gauss law for magnetic field can be written in integral form with

$$\oint_S \bar{B} \cdot \bar{n} da = 0. \quad (14)$$

In order to use these equations a constitutive relation between magnetic field density B and strength H needs to be established. These quantities are linked by permeability μ

$$B = \mu(H)H. \quad (15)$$

This relationship is non-linear as μ is a function of the magnetic field strength and not a constant. Permeability is dependent on the material and it describes material's ability to sustain a magnetic field within its structure.

Different kind of materials act differently when an external magnetic field is forced upon them. The external field causes magnetic dipoles of the material to align themselves with the direction of the field, thus enhancing the field. Domains are created within the material where the magnetic moments of the atoms are parallel with the neighbouring atoms. Domains with different orientations are separated by walls where the direction of the magnetic moment of the atoms is changed. More magnetic dipoles will align themselves in the direction of the magnetic field as the magnetic field strength is increased. This causes the walls between domains to collapse and domains will merge.

Permeability of different materials is usually given as relative permeability instead of absolute permeability according to

$$\mu = \mu_0 \mu_r, \quad (16)$$

where μ_0 is permeability of free space and μ_r is the relative permeability of the material. Permeability of free space is a universal constant and its value is $4\pi \cdot 10^{-7} \frac{\text{Wb}}{\text{Am}}$. Relative permeabilities of magnetic materials range from several hundreds to tens of thousands [15]. The bigger the permeability the better is the ability to sustain a magnetic field.

Materials are usually classified as either diamagnetic, paramagnetic or ferromagnetic. Diamagnetic materials decrease the magnetic field density compared to a vacuum while paramagnetic materials increase the density slightly. Ferromagnetic materials cause a substantial increase to magnetic field density compared to the vacuum.

The chart on the left hand side of Figure 9 shows the BH-curve of materials with different permeabilities. A material can increase the effect of the external magnetic field until it

reaches saturation. At this point all the domains are pointing in the direction of the external magnetic field and increasing the strength of the external field causes only a slight increase in flux density. From this point on the inductor acts as an air cored inductor. In the linear region before saturation, permeability is the slope of the function. The larger the permeability the steeper is the curve.

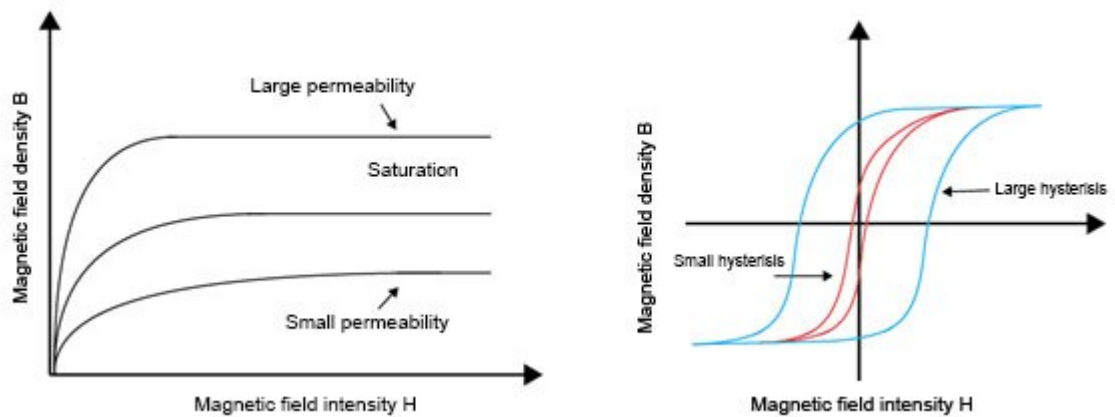


Figure 9 Relationship between magnetic field strength and density. Higher magnetic field density for the same magnetic field strength is present in materials with high permeability. Hysteresis loop for materials with high and low remanence flux.

Once the strength of the external field is decreased, some of the domains still keep their alignment and magnetic field density lags magnetic field strength. Even when the external field is completely removed the material stays magnetized and field density is not zero. This magnetization is called remanence flux. A negative magnetic field is needed in order to demagnetize the material and drive flux density to zero. This effect is called hysteresis. Size of the hysteresis loop is dependent on the coercivity of the material. Materials that have large hysteresis are called hard magnetic materials while materials with small hysteresis are called soft magnetic materials. Permanent magnets are an example of hard magnetic materials.

If an alternating magnetic field is applied a hysteresis loop will be traced out as shown on the right hand side chart of Figure 9. Changing the magnetic field inside the material causes heating and power losses which are proportional to the size of the hysteresis loop. Large hysteresis can be of use in certain applications, but in low-loss magnetic component design materials with small hysteresis loops are preferred.

3.1.2 Magnetic circuit and reluctance

Magnetic reluctance resists the flow of flux and it is equivalent to electrical resistance. The unit of reluctance is $[1/H]$. Reluctance can be defined from Ampere's law. Equation

(10) can be presented using magnetic flux Φ instead of magnetic field strength H in the following form

$$F = \Phi \frac{l}{\mu A} = \Phi \mathfrak{R} = Ni. \quad (17)$$

Reluctance of an element depends on the cross-sectional area, length and the permeability of the material according to

$$\mathfrak{R} = \frac{l}{\mu A}, \quad (18)$$

where l is the length of the element, μ is the permeability of the element and A is the cross-sectional area of the element. It can be seen from (18) that reluctance gets smaller as permeability of the medium increases. The reciprocal of reluctance is permeance

$$P_m = \frac{1}{\mathfrak{R}} = \frac{\mu A}{l}. \quad (19)$$

Properties of the magnetic circuit can be adjusted by adding an air gap to the core. Effects of the airgap are presented in [16]. Air gap reduces the magnetic flux in the circuit, which in turn allows a larger current before saturation. The slope of the Ψ - I curve is less steep and the curve is linearized if an airgap is added. Air gaps are also used to protect the inductor from variation of the core materials permeability. Different batches of the magnetic material might have slightly different values of permeability. Air gap protects the inductor against these variations.

The reluctance of the core and the air gap can be calculated as two separate reluctances according to (20) and (21). These reluctances can be connected in series and added to together. Reluctance of the air gap and the core can be calculated with

$$\mathfrak{R}_{\text{core}} = \frac{l_{\text{core}}}{\mu A_{\text{core}}} \quad (20)$$

$$\mathfrak{R}_{\text{gap}} = \frac{l_{\text{gap}}}{\mu_0 A_{\text{gap}}}. \quad (21)$$

Another way is to calculate the effective reluctance of the circuit which is defined by the ratio of the airgap and magnetic material lengths. Effective permeability for cores with uniform cross-sectional area in the airgap and the core can be calculated with

$$\mu_{\text{eff}} = \left(\frac{\mu_{\text{core}}}{\frac{l_{\text{gap}}}{l_{\text{core}}} \mu_{\text{core}} + 1} \right) \mu_0. \quad (22)$$

Reluctance of the magnetic circuit can be calculated by using the effective permeability and total length of the circuit. Increasing the length of the airgap decreases the effective permeability and increases total reluctance of the magnetic circuit. A gapped core and an equivalent circuit is shown in Figure 10.

Magnetic cores can be more complicated than shown in this figure. In these cases a reluctance network can be created in order to calculate the reluctance of a gapped magnetic core. As shown in (14), sum of magnetic flux through a closed surface is zero. This means that Kirchoff's current law holds true to magnetic flux as well. The flux entering a node must equal the flux leaving the node.

Reluctances of different elements of a core that are in series or parallel can be calculated similarly to resistances in electrical circuits [17]. This way the total reluctance of the circuit can be obtained. However, the permeability of the core is usually thousands of times higher than the permeability of the airgap. In these cases the reluctance of the core can usually be neglected [15]. It is enough to calculate the reluctance of the air gap as most of the reluctance of the magnetic circuit is present in the airgap.

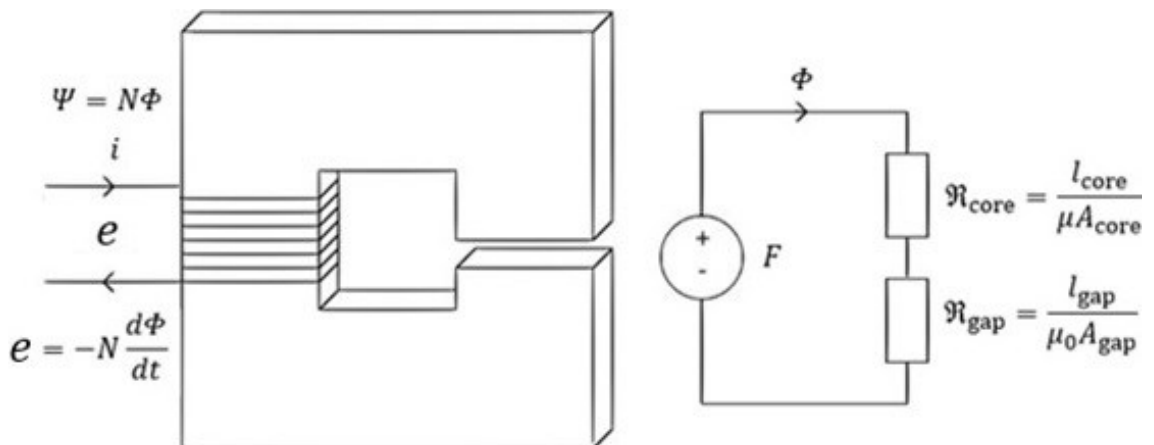


Figure 10 A gapped magnetic core and an equivalent magnetic circuit.

Reluctance depends on the cross-sectional area of the air gap. However flux distribution is not uniform in the air gap. Flux tends to bulge outward thus increasing the air gap area. This effect is called fringing flux and it is depicted in Figure 11. This effect is higher in cores made of materials with low permeability. Fringing flux increases the effective cross-

sectional area and thus decreases reluctance. Depending on the gap geometry and length this can make a major difference when calculating the inductance of the core.

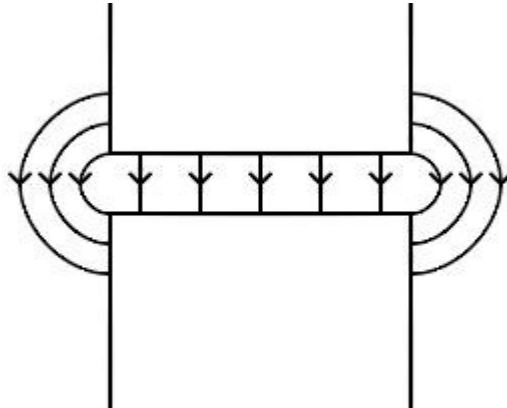


Figure 11 Fringing flux in the air gap. Magnetic flux tends to bulge outward. Airgap dimensions and permeability of the material determine the size of fringing flux.

There are numerous ways to calculate the effects of fringing flux. If the air gap length is small compared to the dimensions of the cross-section of the core, fringing flux effect can be neglected.

A rough estimate of the effects of fringing flux can be made by increasing the air gap area by 10%. A more accurate approximation can be made by adding the length of the air gap to the dimensions of the airgap [18]. For a rectangular core this can be expressed as

$$\mathfrak{R}_{\text{gap}} = \frac{l_{\text{gap}}}{\mu_0(a + l_{\text{gap}})(b + l_{\text{gap}})}, \quad (23)$$

where a is the width of the leg and b is the thickness of the core. For a more accurate estimation a term called the fringing flux factor can be used. Fringing flux factor is the ratio between the flux in the core area and the flux in the same area of the air gap. In an ideal case the fringing factor is unity. Fringing factor can be calculated by equation

$$F_{\text{FF}} = 1 + \frac{l_{\text{gap}}}{\sqrt{A_{\text{core}}}} \ln \left(\frac{2W}{l_{\text{gap}}} \right), \quad (24)$$

where W is the length of the core leg [19]. The inductance value obtained should be multiplied by the fringing flux factor in order to get the correct inductance value.

A more elaborate model for calculating the effect of fringing flux is presented in [20]. The model accounts for different kind of geometries for the air gaps. The flux behaves differently in a corner or a T-junction. In the scope of this thesis such a detailed model is not necessary and the approximation shown in (23) is used.

In most cases fringing flux is not desired as it creates eddy currents into the core material when the flux lines hit the surface perpendicularly. Fringing flux effect can be reduced by splitting the air gap into several smaller air gaps [16].

In powder cores the air gaps are distributed throughout the core. Using these cores eliminates the effects of fringing flux, but these cores are more expensive than regular ferrite or magnetic steel cores. Another way to reduce fringing flux is to place the airgaps inside the windings. This contains the stray flux within the core. In terms of manufacturing the easiest way is to use single gaps between the yoke and the leg, but this increases fringing flux. Splitting the air gap into multiple smaller gaps increases the cost and duration of manufacturing, but yields smaller fringing flux.

3.1.3 Inductance

Inductance links the EMF and derivative of current. The unit of inductance is henry [H]. Inductance can occur through mutual inductance or self-inductance. In the case of chokes inductance is acquired through self-inductance. When a conductor is wound into a coil and current flows through the component, an EMF is created by the variation of the inductor's own magnetic field. This EMF opposes changes in the current according to Lenz's law.

Inductors store energy in their magnetic fields and inductance depicts how much energy can be stored into the magnetic field of the component. When current is decreased energy is released and the inductor opposes the change in current. Voltage over an inductor can be calculated with

$$u_L = L \frac{di_L}{dt}. \quad (25)$$

The voltage drop across the coil is equal to the EMF induced by the magnetic field. Equation for the EMF is defined by Faraday's law and it was introduced in (13). Combining (13) and (25) leads to

$$L \frac{di_L}{dt} = N \frac{d\Phi}{dt} \quad (26)$$

and solving (26) for L yields

$$L = \frac{N\Phi}{i}, \quad (27)$$

which is the definition for self-inductance. (17) is used to calculate the reluctance of the magnetic circuit and it can be solved for magnetic flux Φ . The resulting equation can be inserted to (27) to obtain

$$L = \frac{N^2}{\mathfrak{R}} = N^2 \frac{\mu A}{l}. \quad (28)$$

It can be seen from (28) that inductance depends on reluctance of the magnetic circuit and square of the number of turns. Inductance can be affected by changing either number of turns, area of the core, permeability of the core or length of the magnetic circuit.

Increasing the number of turns yields a higher inductance. For a given amount of current, more MMF is created. Increasing the length of the magnetic circuit while keeping the number of turns same results in a smaller inductance. Longer magnetic path increases the reluctance to magnetic flux. Inductance can be increased by using a high permeability material as core. Inductance also increases if the area of the coil is increased, because a larger area results in less reluctance to the magnetic flux.

Inductance is inversely proportional to reluctance so it decreases as reluctance of the circuit is increased. As mentioned in the previous chapter in most cases it is enough to consider only the reluctance of the air gap and the reluctance of the core can be neglected. Using this approximation inductance of a gapped core inductor can be manipulated by changing the air gap dimensions or number of turns.

Presented equations assume that magnetic flux is uniformly distributed in the core. In reality, not all of the flux lines stay inside the area of the magnetic core. Some stray to different direction and face a path with different reluctance. These flux lines are called stray flux and they create stray inductance. In simple magnetic circuits, stray flux can be neglected, but it is important to be aware of the simplifications while using the presented equations. More accurate estimate of the flux can be calculated using magnetic modelling and finite element method (FEM).

3.2 POWER LOSSES IN A CHOKE

Energy is stored in to the magnetic field of the inductor. All of this energy cannot be recovered as electrical energy and some of it is lost as heat. The power losses of an inductor consist of winding losses and iron losses.

Winding losses occur in the windings due to the resistance of the conductor and they are straightforward to calculate and measure. Iron losses account for rest of the losses that occur in the core and other conductive parts of the inductor due to hysteresis and eddy currents. Iron losses are extremely difficult to predict and measure.

3.2.1 Winding losses

Winding losses are the losses that occur in the coil. These losses are due to the resistance of the coil windings. Electrical energy is dissipated and it appears as thermal energy.

Winding losses are proportional to the square of the current. In high current applications it is the major cause for losses. The winding losses can be calculated with

$$P_{DC} = I^2 R_{DC}, \quad (29)$$

where P_{DC} is the winding loss, I is the RMS-value of current and R_{DC} is the DC resistance of the inductor. The DC resistance can be calculated using equation

$$R_{DC} = \rho \frac{l_w}{A_w}, \quad (30)$$

where ρ is the resistivity of the material, l_w is the length of the conductor and A_w is the cross-sectional area of the conductor. Resistivity depends on the material and it relates the length and cross-sectional area of the object to object's resistance. Resistance of the conductor can be decreased by increasing the cross-sectional area, decreasing the length or changing the material of the conductor.

Losses are also generated by skin effect. Current in the conductor induces circulating currents that force the current to flow closer to the surface. This means that the effective cross-sectional area is smaller than the actual physical area. Skin depth is the depth at where 63% of the current flows. For low frequency cases skin depth can be calculated with equation

$$\delta = \sqrt{\frac{2\rho}{\omega\mu}}, \quad (31)$$

where $\omega = 2\pi f$. It can be seen that skin depth is affected by frequency. Skin depth gets smaller as the frequency is increased. Flux lines, striking the windings perpendicularly, cause circulating eddy currents in to the windings that cause excess heat and resist the flow of useful current. Skin effect is non-existent in the case of DC current and for 50 Hz AC-current the skin depth is 8,5 mm for copper and 10,5 mm for aluminium. Increasing the radius of the conductor wire beyond these quantities is not effective. At higher frequencies skin effect needs to be taken into account, otherwise material will be wasted.

Proximity effect can be seen in windings with multiple turns wound into a tight coil. Current flowing in the adjacent conductors create magnetic fields that in turn create eddy currents that force current to flow in the conductor. This current crowding causes a smaller cross-section to be used, hence increasing resistance. This effect can also cause excessive heating of the conductor. Proximity effect can be decreased by reducing the number of turns and layers. Losses caused by proximity effect are also dependent on frequency. At low frequencies proximity effect can be neglected [21].

Total AC winding loss consists of the DC losses, eddy current losses and skin effect losses according to

$$P_{AC} = P_{DC} + P_e + P_s. \quad (32)$$

This equation applies to high frequency AC applications where skin effect and eddy currents contribute to a big part of the total losses. In DC or low frequency 50 Hz applications that utilize a simple diode bridge for rectification the skin effect and eddy current losses are basically negligible. In these cases winding losses can be approximated to be equal to losses caused by the DC resistance [21].

3.2.2 Iron losses

Iron losses occur in the core or other conductive parts of the inductor. Main reasons for the core losses are hysteresis and eddy currents. There is also residual loss that can't be directly placed under any category.

Hysteresis losses depend on the level of magnetic induction. In the case of AC chokes the current and magnetic flux alternate between the peak values and a hysteresis loop similar to Figure 8 is drawn out. The hysteresis loss of the choke can be seen in the BH-curve. The area between the curves is equal to the energy lost during one cycle [22]. If B and H are measured at an arbitrary point in the core the hysteresis loop consist of only hysteresis losses. Eddy current and residual loss are included in to the loop if average flux density throughout the whole core is measured. Total hysteresis power loss can be calculated by multiplying the energy lost during one cycle by frequency.

The higher the frequency, the higher the amount of cycles. This results in increased losses. In addition to the major hysteresis loop, minor loops are caused due to ripple in current. In the case of DC chokes, a constant level of DC current and flux is present at all times. Ripple effects are added on top of this DC bias. This results in minor hysteresis loops at the DC bias.

Eddy currents are circulating currents that appear according to Faradays's law. The core acts as closed circuit and circulating currents start to flow in the core. The magnetic field induces a current, which in turn creates a magnetic field that opposes the original field.

Magnetic cores are usually made from iron alloys which are good electrical conductors. Small resistance of the core increases eddy currents. Skin effect was discussed in relation to winding losses, but it also plays a role in iron losses. In order to reduce the amplitude of eddy currents, the cores can be stacked up from thin laminated sheets. Another method is to use core materials with higher resistivity. These cores are usually more expensive and can support lower flux densities.

Core losses are usually given by manufacturers as charts indicating power loss per volume. Core losses are extremely difficult to calculate. Core losses under sinusoidal excitation can be evaluated by the Steinmetz's equation

$$Q_v = kf^\alpha B^\beta, \quad (33)$$

where Q_v is loss per volume, B is maximum field density and f is excitation frequency, k , α and β are material dependent parameters [23].

3.3 DESIGN OF MAGNETIC COMPONENTS

Multiple things need to be taken into account when designing magnetic components. The application of the choke sets design constraints that set boundaries to the design. Different design constraints and aspects are given in the following sections. Theory of magnetic properties was introduced in the previous section, while this section provides a more practical equations for determining the correct core dimensions, air gap lengths and number of turns. Equations for calculating maximum flux density and saturation current are presented. Thermal behaviour and IP protection classes are also introduced.

3.3.1 Design constraints

Several constraints drive the design of magnetic components and depending on the application, different aspects are more important than others. Usually the inductor is wanted to operate in the linear region so that fluctuations or peaks in the current won't affect the inductance of the choke. This means that the peak current shouldn't drive the core to saturation. Core power losses is also an important constraint. In the case of DC chokes or 50 Hz AC chokes, saturation current is usually the dominating constraint [16]. Saturation current can be increased by increasing the core area of the choke, using a magnetic material with higher maximum flux density or by adding air gaps in to the core.

Winding losses should be kept as low as possible. This calls for a large cross-sectional area for the conductor and as few turns as possible. On the other hand increasing the wire size increases the amount of space needed. And cutting down the number of turns means that either cross-sectional area of the core needs to be increased or the length of the air gaps needs to be decreased. Increasing the core cross-sectional area takes up even more space and decreasing the air gaps can increase the flux density above saturation limit. Outer dimensions of the choke are dictated by the free space inside the frame of the converter. In certain applications the weight of the choke might be an important factor. Winding losses are reduced as the core size is increased up to certain point. After that point the mean path length (MPL) of the wire is so long that the reduced number of turns won't help.

No matter how tight the wires are wound there will be empty space between the wires. The total copper area is always smaller than the total winding window. The empty space can be utilised better with square or rectangular wire than with round wire. Insulation takes some of the space and clearance to the adjacent windings have to be taken in to

account also. A proper clearance needs to be left at the ends of the leg. The leg needs to be attached to winding machinery and there needs to be enough space for the attachment.

3.3.2 Calculating inductance and saturation current

Inductance of the choke can be calculated by (28). There are multiple unknown variables and it might be time consuming to just start trying different values. It is helpful at first to approximate that all the reluctance of the magnetic circuit is in the air gap. The amount of energy needed to be stored in the air gap of the choke is then

$$W_{\text{gap}} = \frac{1}{2} L I_{\text{peak}}^2, \quad (34)$$

where I_{peak} is the maximum current passing through the choke during operation. Energy stored in the airgap can be used to calculate the needed length of the air gap. According to [24] the field energy of the choke can be calculated with

$$W_{\text{field}} = \frac{1}{2} \int H B dV, \quad (35)$$

where W_{field} is the field energy and V is the volume of the air gap. If a uniform flux density distribution is approximated and the reluctance of the core is neglected, (34) and (35) can be presented as

$$\frac{1}{2} H_{\text{gap}} B_{\text{gap}} V_{\text{gap}} = \frac{1}{2} \frac{B^2}{\mu_0} l_{\text{gap}} A_{\text{gap}}. \quad (36)$$

Equation 36 can be solved for the airgap length as follows

$$l_{\text{gap}} = \frac{W_{\text{gap}}}{\frac{1}{2} \frac{B^2}{\mu_0} A_{\text{gap}}}. \quad (37)$$

Maximum allowed field density can be inserted into (37) in order to obtain the air gap length that allows the core to function without saturating. Once the required airgap length is known, the required number of turns can be calculated by solving (28) for N

$$N = \sqrt{\frac{L l_{\text{gap}}}{\mu_0 A}}. \quad (38)$$

Both the airgap length and number of turns need to be rounded. Due to rounding and approximations in the equations, it is necessary to check the inductance, maximum field density and saturation current of the choke. The choke must be designed so that the maximum peak current doesn't drive the core in to saturation. Usually a margin of 10% or

more is used due to component aging, current spikes and other interference. AC ripple might cross the saturation current even if the fundamental or DC current stays below it. Maximum field density of the choke can be calculated by inserting the peak current to

$$B_{\max} = \frac{LI_{\text{peak}}}{A_c N}. \quad (39)$$

If the saturation field density of the core material is known, saturation current can be calculated with

$$I_{\text{sat}} = \frac{B_{\text{sat}} l_{\text{gap}}}{\mu_0 N}. \quad (40)$$

If necessary the number of turns or airgap length can be fiddled with. Increasing the air gap length decreases inductance. Flux density is smaller for a given field strength which means that a higher current can be applied before the saturation of the core. According to (18), smaller permeability increases the total reluctance of the circuit and inductance is decreased. In order to maintain the initial inductance value the number of turns must be increased. However, increasing the number of turns will also increase the magnetic field strength H and thus magnetic flux density B . It can be seen from (10) and (28) that magnetic field strength H is directly proportional to the number of turns while inductance is proportional to the square of the number of turns.

3.3.3 Thermal behaviour

Heat transfer is an important part of choke design. High temperatures require higher thermal class which increases cost. Increased temperatures can also cause degrading in other components. Low resistivity results in smaller power losses and thus a smaller thermal energy heating the component.

Heat is transferred from the choke by convection, conduction and radiation. Convection requires a coolant like air or fluid and it can be forced or natural. Conduction takes place between or within solid materials. Radiation requires no medium. Radiation and convection account for the majority of heat transferred in traditional choke designs. Forced air cooling increases the effect of convection. Cooling capability of the choke can be evaluated by calculating the thermal resistances of different parts of the choke and by building a thermal network. Different heat transfer methods are presented in Figure 12.

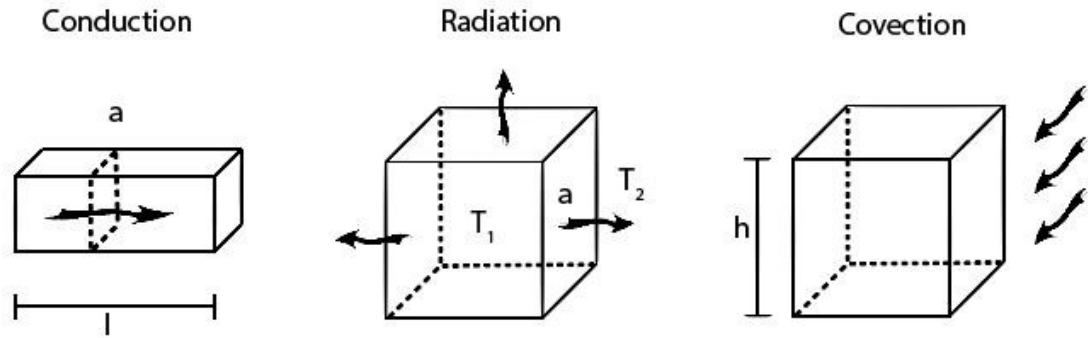


Figure 12 Heat can be transferred either by conduction, convection or radiation..

Thermal resistance of conduction for a simple cubical object can be calculated with

$$R_{cd} = \frac{\Delta T}{P} = \frac{l}{A\lambda}, \quad (41)$$

where ΔT is the change in temperature, P is the heating power, l the length of the object, A is the cross-sectional area of the object and λ is heat conductivity of the material. Thermal resistance of radiation for an object with emissivity ϵ_1 can be calculated with

$$R_r = \frac{\Delta T}{P} = \frac{T_1 - T_2}{\epsilon_1 \sigma (T_1^4 - T_2^4) A_1}, \quad (42)$$

where ϵ_1 is the emissivity of the radiating object, A_1 is the surface area of the radiating object T_1 is the temperature of the radiating object, T_2 is the temperature of the absorbing object and $\sigma = 5,67 * 10^{-8} \frac{W}{m^2K^4}$ is the Stefan-Boltzmann constant. Thermal resistance of convection can be calculated with

$$R_{cv} = \frac{\Delta T}{P} = \frac{1}{h_c A}, \quad (43)$$

where h_c is the heat transfer coefficient for convection. Empirical equations for calculating heat transfer coefficients for natural and forced convection are given in [25]. Natural convection heat transfer coefficient can be calculated with

$$h_c = 1,42 \left(\frac{\Delta T}{l_h} \right)^{0,25} \quad (44)$$

where l_h is the vertical height of the component. Forced convection heat transfer coefficient can be calculated with

$$h_c = \frac{3,33 + 4,8v^{0,8}}{l_c^{0,288}}, \quad (45)$$

where v is the velocity of the flowing air and l_c is the total distance passed by the air cooling the component.

Using these thermal resistances a thermal network can be built and the temperature change can be evaluated. Simplified thermal model can be created by assuming that the hot spot is in the windings and that the temperatures within the windings and core are uniform. This simplified model then accounts for heat transferring from the wire to the core by conduction and radiation and to the ambient by radiation and convection. On top of that heat is transferred from the core to the ambient by convection and radiation [25]. Thermal network is presented in Figure 13.

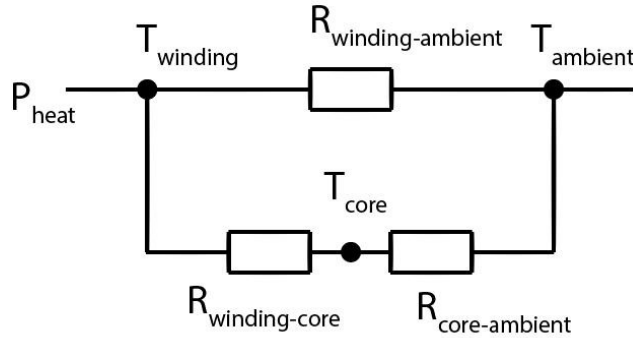


Figure 13 Simplified thermal network. Hotspot is in the winding and temperatures are uniform inside the windings and the core.

A rough estimate of the temperature rise for C-core or toroidal inductors can be calculated with

$$T_r = 450 \left(\frac{P}{A_t} \right)^{0.826}, \quad (46)$$

where P is the total power dissipated by the inductor and A_t is the effective surface area of the inductor [19]. This is an empirical equation that assumes emissivity of 0.95 and that 45% of the heat transfer is due to convection and 55% is due to radiation.

Resistance of a material is not constant. It changes with the temperature according to

$$R_T = R(1 + C_m(T - T_0)), \quad (47)$$

where R is the resistance of the material in the initial temperature, C_m is the temperature coefficient of the material and T_0 is the initial temperature [26]. (47) can be solved for T in order to evaluate the temperature at given resistance

$$T = \frac{R_T - R + RC_m T_0}{RC_m}. \quad (48)$$

Average temperature of the windings can be calculated with (48) by measuring the voltage over the windings at different DC currents. Even a low resistance design can exhibit high losses if it doesn't cool properly.

Mass, surface area and material of the object affect the cooling and the time constant of the object. Time constant describes how quickly the object reacts to temperature changes. Time constant τ describes the time it takes for the object to reach 63% of the target value. The smaller the time constant, the faster the object reaches thermal equilibrium.

Thermal classes for insulating materials are introduced in IEC 60085 Standard. They give maximum hotspot and average winding temperatures for different classes. Thermal classes for electrical insulation are presented in Table 6.

Table 6 Thermal classes of insulating materials [27]. Limits for maximum hot spot temperatures and temperature rises are given.

Thermal class	Previous designation	Hot spot allowance	Permitted design temperature rise	Permitted average winding temperature determined by resistance measurement
90	Y	90	-	-
105	A	105	60	-
120	E	120	75	-
130	B	130	80	120
155	F	155	100	140
180	H	180	125	165

Insulation of the choke has to be chosen according to the results of thermal analysis. Insulating material for high thermal classes are more expensive than for lower classes.

3.3.4 IP-class

Protection against the environment has to be taken into account when designing a choke. IP-class is a universal protection standard that consists of two numbers. The first number describes protection against solid particles and dust and the numbering ranges from 0 to 6. The second number describes protection against water and values range from 0 to 8. The higher the number, the better the protection. Description for different codes are shown in Figure 14.

Ingress Protection (IP) According to EN 60529 / DIN 40050					
IP68 Protection Against Dust			IP68 Protection Against Water		
0	No protection	No contact protection, no protection against solid particles and foreign bodies.	0	No protection	No protection against water.
1	Protection against large foreign bodies	Protection against large contact area with hands and foreign bodies $6 > 50\text{mm}$.	1	Protection against dripping water	Protection against vertical water drops.
2	Protection against medium foreign bodies	Protection against contact with fingers, protection against foreign bodies $6 > 12.5\text{mm}$.	2	Protection against inclined water drops	Protection against inclined water drops (any angle up to 15° to vertical line).
3	Protection against small foreign bodies	Protection against tool contact foreign bodies, wires or the like with $0 > 2.5\text{mm}$.	3	Protection against spray-water	Protection against spray water from an angle of 60° to vertical line.
4	Protection against foreign grains	Protection against tool contact, foreign bodies, wires or the like with $0 > 1\text{mm}$.	4	Protection against splash-water	Protection against splash water from all directions.
5	Dust-protected	Full contact protection. Protection against dust deposits inside.	5	Protection against water jets	Protection against water jets from any angle.
6	Dust-tight	Full contact protection. Protection against dust penetration.	6	Protection against powerful water jets	Protection against powerful water jets from any angle.
			7	Protection against immersion	Protection against water penetration 1m below the surface.
			8	Protection against submersion	Protection against pressure water for an indefinite time (customer tailored).

Figure 14 Chart of different protection classes [28]. The first number describes the protection against solid particles and dust and the second number describes protection against water.

There are multiple ways to create protection for the chokes. A layer of felt can be wrapped around the conductor of the choke. The choke is then treated with resin multiple times and the felt absorbs the resin thus creating a water resistant protective layer. Insulating paper which absorbs the resin can also be used. A more thorough way is to use a plastic shell around the conductive parts that is sealed at both ends. This creates a capsule that is water- and dustproof. A more advanced method is to pot the choke with materials like epoxy or polyurethane. The potting material can be chosen based on the application. It can be used to guarantee for example electric insulation, waterproofing or thermal conductivity. High IP-class requirement can hinder the thermal cooling of the choke.

3.4 CORE DESIGN

Core of the choke is made of magnetic material that enhances the magnetic field. High permeability and flux density are desired in order to keep the choke size small. Air cored chokes can also be used, but large inductances can't be reached without considerable increase in choke size. Core material of the inductor must be chosen according to the operating conditions and specification of the design. An ideal material would have linear permeability, small power loss and high saturation density. Unfortunately one cannot have all of these properties simultaneously and optimization needs to be done.

3.4.1 Core materials

An overview of magnetic materials used is given in [29] and [30]. Ferrite cores are used for high frequency designs due to their high resistivity. Maximum flux density is low for ferrites, usually in the range of 0,3-0.5 T. For this reason they are not commonly used in line or link choke applications. Most common ferrites used are Manganese-Zinc (MnZn) and Nickel-Zinc (NiZn) ferrites.

Magnetic steel is the most common core material for chokes. Magnetic steel is usually made from silicon-iron (SiFe) alloy, but other alloys like cobalt-iron (CoFe) and nickel-iron (NiFe) alloys are also used [30]. Magnetic steel allows relatively high flux densities before saturation. Maximum flux density of 1,2 T is common for SiFe alloys while flux densities over 2 T can be achieved with CoFe alloys.

Magnetic steel is very conductive so cores must be stacked from laminated sheets in order to reduce eddy currents even at low frequencies. The thickness of the sheets is usually below 1 mm. Each of the sheets is insulated in order to hinder the flow of eddy current. Stacking and lamination thickness reduce the effective magnetic area of the core. A stacking factor is given by the manufacturer which can be used to calculate actual magnetic core area. Magnetic steel is manufactured with different specifications and ratios. Some materials allow higher maximum flux density while others aim for smaller losses. Material should be chosen according to the application.

Magnetic steel can be grain oriented. In non-oriented (*NO*) steel the grains are pointing in random directions and the steel sheet has similar magnetic properties in every direction on the plane of the sheet. Grain oriented (*GO*) steel is manufactured so that all grains are pointing in the direction of the rolling. *GO* steels have great magnetic properties in the direction of the rolling. However magnetic properties in the traverse direction are weakened. Due to the manufacturing process, *GO* steels have slightly higher content of Si. The resistivity of *GO* steel is thus higher. In applications where the direction of the magnetic flux can be guaranteed, *GO* steel can be used to boost the properties of the inductor. However *GO* steel is much more expensive than *NO* steel [31]. Using *GO* steel might take few turns off the windings so the total cost effect must be calculated.

Soft magnetic composites (*SMC*) are iron powder cores that are made of small isolated iron particles. *SMC* cores are solid objects and not made from stacked sheets. The structure of the material increases resistance and thus decreases eddy currents. Usually air gaps are not needed which reduces the fringing flux effect to minimum. Powdered cores allow flux densities up to 1,0 T. Different types of alloys and material ratios can be used to acquire different permeabilities, power losses and saturation flux densities. Powder cores have lower permeability than ferrites but they can stand more current without saturation. Powder cores are more expensive than *GO* or *NO* steel cores.

Amorphous and nanocrystalline cores are among non-conventional core materials. Unlike other steel sheets, amorphous material is usually produced by melt spinning. This results in a very thin foil-like structure that doesn't have crystalline structure like other magnetic materials. Typical thickness for amorphous material is only around 0,025 mm [29]. Resistivity of amorphous materials is high which reduces eddy currents effectively. Due to the thinness of the material, amorphous cores are usually tapewound or premanufactured into stacks. Nanocrystalline materials are manufactured in the same way as amorphous materials. Nanocrystalline materials have very small grain size and the metallurgical

structure of the material is very complex. A common nanocrystalline material is an alloy that contains iron, copper, niobium, silicon and boron [30]. Nanocrystalline materials offer higher permeability and maximum flux density than amorphous materials but due to their structure, they are more brittle.

3.4.2 Shape of the core

Core shape can be adjusted according to the application. Shell and core type are the most common ways. In core type inductors the flux lines are flowing in one direction and the magnetic flux density has the same value in every part of the core. In shell type inductors flux lines are split between the two side legs. The core area of the side legs can be 50% of the core area of the centre leg. Flux density will still have roughly the same value throughout the core. If equal sized airgaps are on the centre leg and the side legs, the total airgap reluctance of the circuit equals two times the airgap reluctance of the centre leg. The core of the choke can also be circular or toroid shape. Core type inductor is presented on the left hand side and shell type inductor on the right hand side of Figure 15.

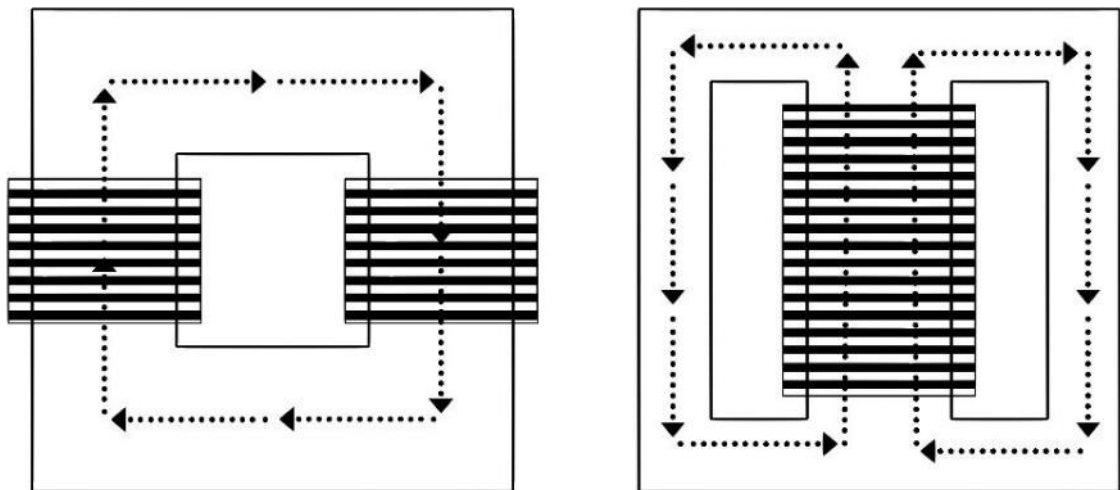


Figure 15 Core and shell type inductors. Direction of the magnetic flux is presented by the dashed arrows.

Cores can be manufactured by different shaped sheet metals. Cut sheets can be in I, U, E or C shape. Creating the core by just I-sheets takes more labour but there is no waste created in the cutting process. Standard sized EI- and UI-cores can also be cut without losing any material in the process. This is an important aspect when calculating to cost of the choke.

3.5 WINDING DESIGN

In the case of DC chokes, most of the power losses occur in the windings of the choke. These losses can be minimized by using different winding materials and winding methods. Current density shouldn't rise too high in the material. Weight and cost are important factors when considering feasibility of different solutions.

3.5.1 Winding materials

Most common winding materials are copper and aluminium. Winding material needs to have low resistivity in order to keep the DC losses down. However higher resistivity can reduce eddy current losses. In high frequency operation, a bit higher resistivity can be of advantage. Besides power losses the weight and cost of the choke are important parameters. Basic properties of aluminium and copper are presented in Table 7.

Table 7 Properties of aluminium and copper [32, 33] .

	Aluminium	Copper
Resistivity ($\mu\Omega\text{m}$)	2,65	1,67
Density (g/cm^3)	2,70	8,92
Temperature coefficient of resistance ($\text{ppm}/^\circ\text{C}$)	4308	4027
Thermal expansion coefficient ($\mu\text{m}/^\circ\text{C}$)	23,86	16,7
Price ($\text{€}/\text{kg}$)	1,65	5,11

Copper has low resistivity compared to aluminium. Resistivity of aluminium is 58 % higher than the resistivity of copper. In order to keep the DC power losses at a same level, the cross-sectional area of an aluminium wire has to be 58 % bigger compared to the copper wire. However the density of copper is a lot higher than that of aluminium. In terms of mass, smaller amount of aluminium is needed to achieve the same power loss. In terms of mass, only 47 % of aluminium is needed to achieve the same conductivity. Aluminium wire will take up more space, but total winding mass is actually smaller.

Price of copper and aluminium change constantly based on the commodity markets. Market prices for aluminium and copper are presented in figure 13. At the time of inspection copper was roughly three times as expensive as aluminium. When this is combined with the fact that the same conductivity can be achieved with 47 % less material, aluminium is a really tempting option.

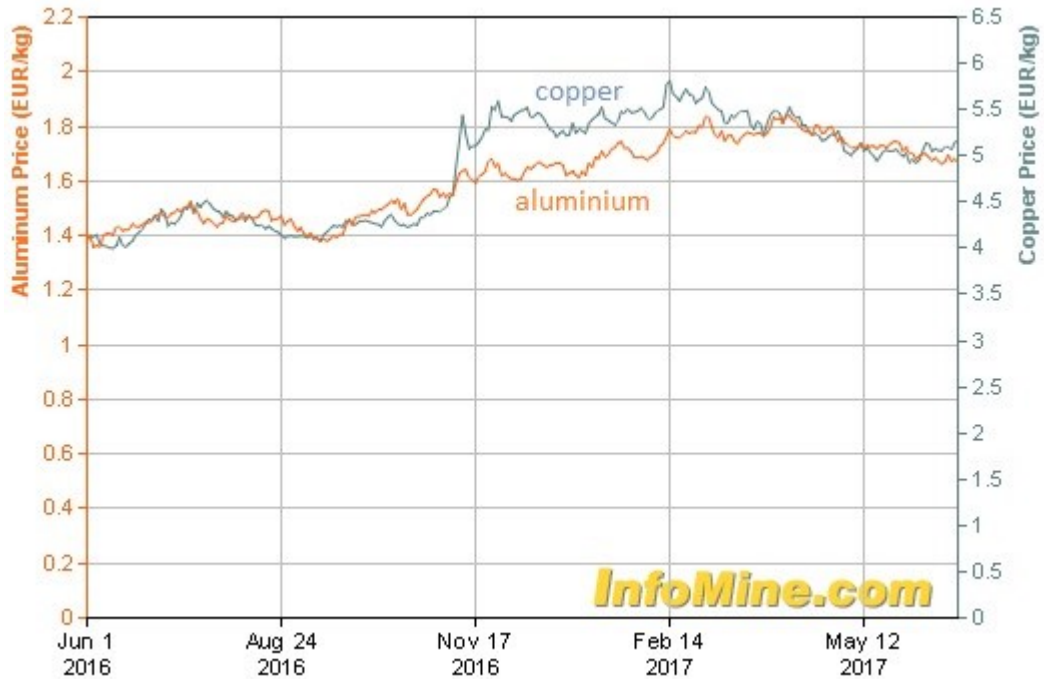


Figure 16 Aluminium and copper prices June 1, 2016 – June 23, 2017 [32].

However copper has other advantages. Termination of aluminium wires is a lot harder than with copper. This is due to the high thermal expansion of aluminium which loosens contacts. Aluminium has also a tendency for rapid oxidation which increases resistivity in the loosened contacts. Contact greases or lubricants can be used to prevent the oxidation. High temperatures can occur in the terminations if they are not done properly. This somewhat increases the cost of aluminium windings [33].

3.5.2 Winding methods

Various winding methods can be used to create inductors. Windings can be wound in to a single or multiple layers and wires can be round or rectangular. It is worth noting that adding multiple layers increases the MPL. Especially with thick wire and a big number of turns, the increase can be substantial. The longer the MPL, the bigger is the resistivity of the wire. Adding layers decreases the amount of core material, but it slightly increases losses due to added length. As discussed before proximity effect can cause high losses in high frequency applications if multiple layers are used. In DC and low frequency cases these losses are negligible. Different winding methods are presented in Figure 17.

Round wire is the most common wire type used. It is cheap and readily available in different sizes in both copper and aluminium. Most manufacturers have machinery that supports different diameters of round wire. Due to the geometry of the round wire, a lot of space is wasted. In the case of multiple layers, the winding can be wound into a helix in order to obtain a tighter fit.

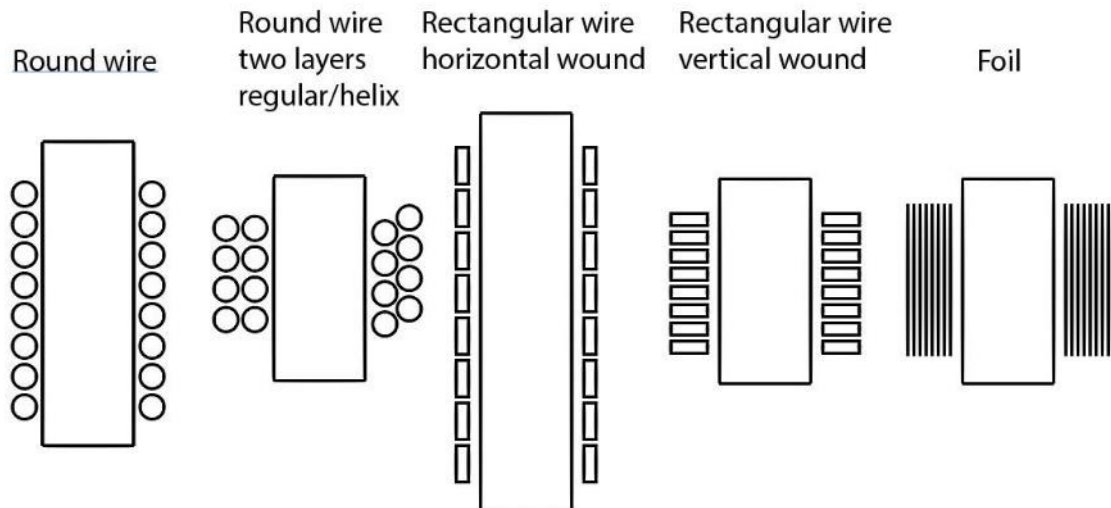


Figure 17 Each picture has 8 turns wound around the core with different winding methods. Cross-sectional area of the wires is the same in every picture.

Rectangular wire can be used to achieve a larger cross-sectional area for the conductor. This wire is a bit more expensive than round wire but they are also readily available in standard sizes for both copper and aluminium. Rectangular wire is usually wound with the longer side down as the wire bends easily in that direction. Rectangular wire can also be wound vertically with the short side down. This requires a bit more room in the winding window but allows the same number of turns around a smaller core length.

Vertical winding method sets limits to the dimensions of the rectangular wire. Tests performed at the choke manufacturer have revealed that with conductor dimensions exceeding 13 mm in width, the insulating coating of the wire starts to tear if the conductor is wound vertically. Winding the rectangular wire vertically requires a lot more strength than if it was wound horizontally. The thickness of the wire is thus restricted by the capability of the machinery. Aluminium is softer than copper and it can usually be wound directly over the fiberglass spacers. Copper is a harder material and fiberglass spacers are not able to endure the force needed to bend the copper vertically. Vertical winding of a copper wire needs a separate coil former. The radius of the turn will also be somewhat larger than with aluminium. This means that aluminium can be wound to a tighter fit and it requires smaller space than copper. The advantage of vertical winding is the possibility to reduce the amount of core material without increasing the MPL of the wire.

Foil is especially good for DC and low frequency applications. Aluminium foil is by far the most cost effective way to manufacture the windings. Aluminium foil comes in different thicknesses and widths. Thickness can vary from 0,5 mm up to 3 mm. Choke manufacturers have standard sizes that they are using but custom strips can be manufactured if necessary. Copper foil is not commonly used which means that it is not as readily available as aluminium foil. Manufacturers don't usually have it in stock and ordering small batches is expensive. This increases the cost difference between the two materials even

further. The foil is wound into multiple layers with an insulator between layers. Usually paper based insulation like Nomex is used. Using foil allows a big cross-sectional area for the wire. It is noteworthy that increasing the number of turns or the thickness of the foil increases the MPL of the wire.

A completely new winding method is presented in appendix B. This winding method aims to maximize the conductor area and utilize the winding window to the fullest. It is aimed especially for low frequency designs. In high frequency applications the added thickness and area of the material do not help due to skin effect.

4. DESIGN OF A NEW DC-CHOKE

The design process of a new choke consists of multiple phases that require utilizing the information presented in the previous sections. Target values are set for the most important parameters that act as the baseline for the design. During the design process compromises need to be made and clear objectives and priorities help guide the process. On top of the objectives, design constraints depending on the application set boundaries to the design. The design can be optimized within these boundaries in order to obtain the best possible solution. Multiple iterations might be needed before the optimal solution is found.

This section presents the baseline for the design process and a brief introduction to the existing chokes that are used as reference for the design. An overview of the design procedure is presented, as well as the Matlab-script that is used for optimizing the design for different variables.

4.1 BASELINE AND OBJECTIVES FOR THE DESIGN

Baseline for the design is an existing DC-choke. Specification for the DC-choke is given in Table 8.

Table 8 Specification of the reference DC-choke.

Nominal current	423 A
Saturation current	700 A
Inductance	64 μ H
Core material	Non-oriented magnetic steel M470-50A
IP-class	IP55

4.1.1 Objective of the design

Aim of the design is to create a new DC-choke that has as low losses as possible while having the same inductance and saturation current as the reference DC-choke. The emphasis is on different winding methods. For this reason the same core material is used. This allows a more straightforward comparison between different designs.

On top of the target values given in Table 8, there are some design constraints that need to be addressed. The choke should fit the existing space reserved in the frame of the frequency converter. This means that the maximum outer dimensions for the choke are

strictly set. Different kind of core shapes and sizes as well as winding methods can be incorporated as long as the maximum width, length or height are not exceeded. Preferably the existing mounting points should be utilized.

Another constraint is the cost of the choke, which consist of material and manufacturing cost. The new design shouldn't exceed the price of the original choke and the weight of the choke shouldn't increase excessively. With so many constraints the objectives need to be prioritized. It is not possible to achieve every single objective. Priority list for the goals is as follows

1. Low power losses
2. Low cost
3. Low weight
4. Utilize existing mounting points.

In the case of conflict between objectives, the objectives with the highest priority will be optimized at the expense of objectives with lower priority.

4.1.2 Reference chokes

Inductance of the reference chokes is measured with a pulse tester. A constant DC voltage is applied to the test inductor, which corresponds to the inductor's real operational conditions. This will result in a current ramp in the test component, whose di/dt slew rate is subject to inductance.

DC resistance of the reference chokes is measured in two ways. A micro-ohm meter DO-7 is used to measure the resistance at room temperature. DO-7 supplies a 10 A current through the choke and calculates resistance based on measured voltage. In addition to micro-ohm meter, resistance is also calculated by applying a much higher DC current of 300 A through the choke with a power supply and measuring the voltage at the coil terminals with a multimeter.

Finally the thermal behavior of the reference chokes is studied by installing the chokes to the frame of the frequency converter and passing nominal current through the chokes. Normal ventilation of the frequency converter is used during the measurement.

The frequency converter in question is manufactured at the moment with two identical 64 μH DC-chokes. The choke is a core-type choke with 22 turns of rectangular 4,5x10 mm copper wire. Core area of the choke is 1470 mm^2 . Core material of the choke is magnetic steel M470-50A. There is also an AC-choke variant that has three coils wound on a common three-legged core. Inductance of each phase is 58 μH . Each winding is made with 10.5 turns of 1x120 mm aluminum foil. The core-area of the choke is 3430 mm^2 .

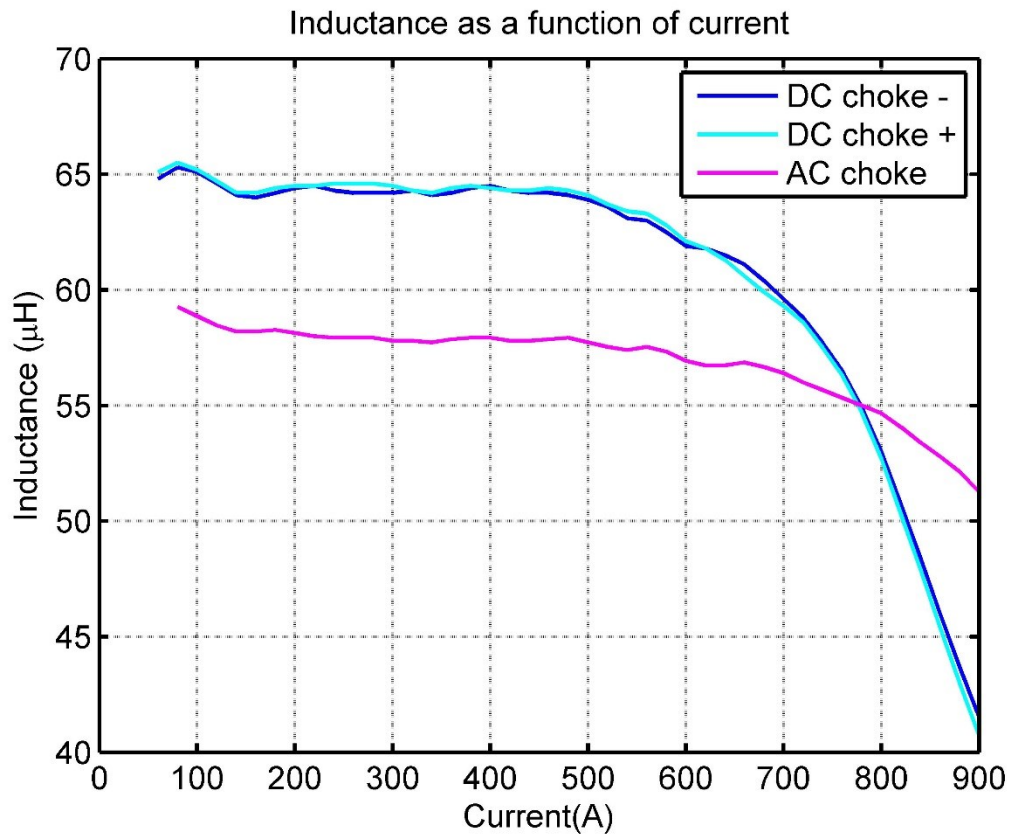


Figure 18 Inductance as a function of current for the reference DC-chokes and the reference AC-choke variant. The reference DC-chokes have a slightly higher inductance while the AC-choke has a larger saturation current.

Inductance curves of the reference DC-chokes and the reference AC-choke are presented in Figure 18. Chart reveals that the AC-choke has a slightly smaller inductance, but the saturation current is higher than with the DC-choke. Inductance of the new designs should behave the same way as the original DC-choke.

Measured resistances of the windings of the reference chokes are presented in Table 9. Winding resistance of the AC-choke is 38 % less than the winding resistance of the DC-choke.

Table 9 Winding resistance of the reference chokes at room temperature measured with two different methods.

Measurement	DC-choke	AC-choke
Micro-ohm meter	1,370 mΩ	0,856 mΩ
Current source and voltage measurement	1,366 mΩ	0,848 mΩ

Resistance of the windings is measured in room temperature. Resistance of the windings increases as the temperature increases. Measured resistances can be scaled to high temperature in order to evaluate power losses at operation temperatures using (47) presented on page 32.

A heat test is performed for the reference chokes. The chokes are installed into a frequency converter with working fans and ventilation. Nominal current of 423 A was fed through the windings. Temperature of the windings is measured with a thermometer and voltage between the terminals is measured with a multimeter. Resistance at different temperatures can be calculated based on the measured voltages and current. Average temperature of the windings can then be calculated based on the resistances using (48) presented on page 32. Average temperatures of the reference chokes are presented in Figure 19.

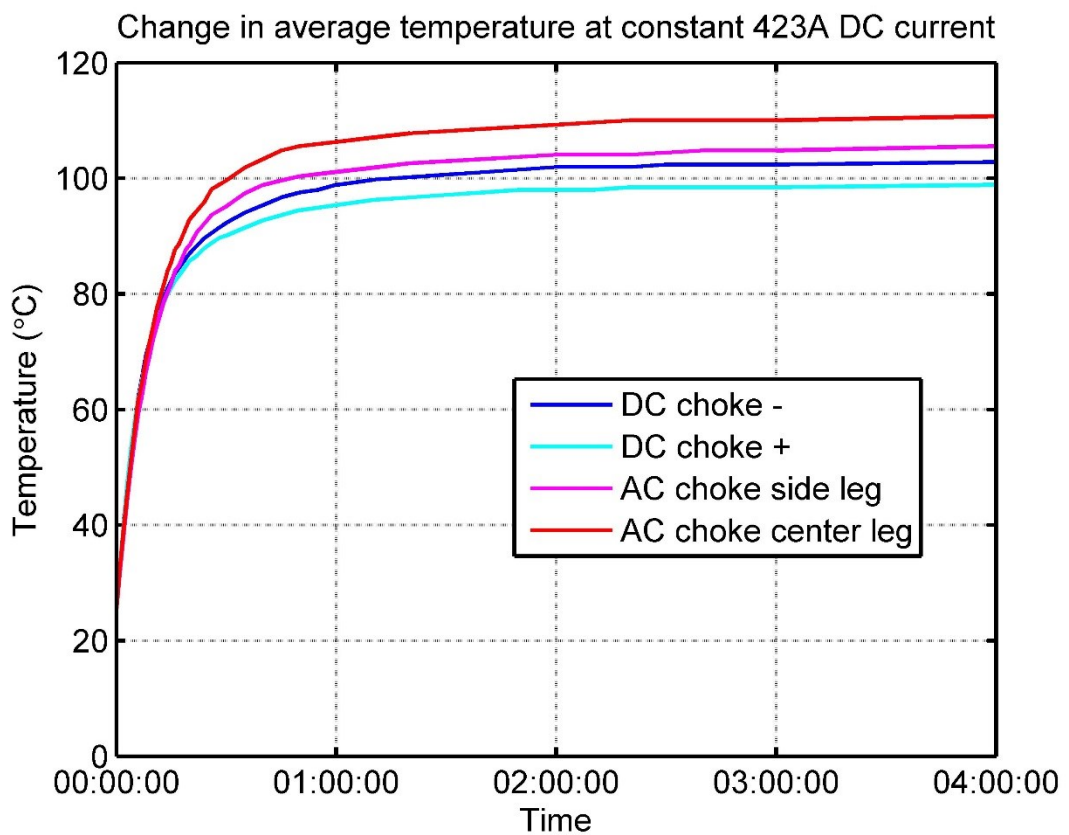


Figure 19 Thermal behaviour of the reference DC-chokes and the reference AC-choke variant at 423 A.

The average temperature in the windings of the AC-choke is somewhat higher than the average temperature in the windings of the DC-choke. Centre leg of the AC-choke has a higher average temperature than the side legs due to the location.

4.2 DESIGN PROCESS

Subsection 4.2.1 presents the flowchart of the design process. Matlab is used to calculate the inductance and resistance of the designs. Result of the simulation is compared to the

measured results in order to validate the script. Matlab scripts used in the design are given in subsection 4.2.2.

4.2.1 Design flow

The design process starts by addressing the system specifications. A proper core material is chosen for the application. In high power frequency converter applications, the saturation current needs to be high. This demands either a material with a high saturation flux density, a big cross-sectional area for the core or large airgap.

Magnetic steel has a high saturation flux density and it is by far the least expensive of the material options. Materials with lower saturation flux densities could be used but the cross-sectional area would need to be increased excessively. This would mean a bigger volume of material that is more expensive. The upside would be lower per volume losses of the material. However the core losses are small compared to the winding losses in the case of DC-chokes.

After core material has been chosen an initial decision about winding material needs to be done. Winding material can be switched after the design process, but a design optimized for one material is not necessarily optimal for the other. Core dimensions determine the core cross-sectional area and winding window area. Winding dimensions and winding window area determine how many turns can be used to build the choke.

Number of turns and air gap length that satisfy the inductance and maximum flux density requirements need to be calculated. At this point it is necessary to check that maximum flux density does not saturate the core. Once it has been established that the design is magnetically feasible, power losses of the choke need to be calculated. Finally thermal and weight calculation are done. Flow chart of the design process is given in Figure 20.

If the necessary requirements cannot be met at any point during the design process, design has to be taken back to the previous phase or even further. Once every step in the flow chart is passed the design can be taken into a more detailed examination in order to finalize the design.

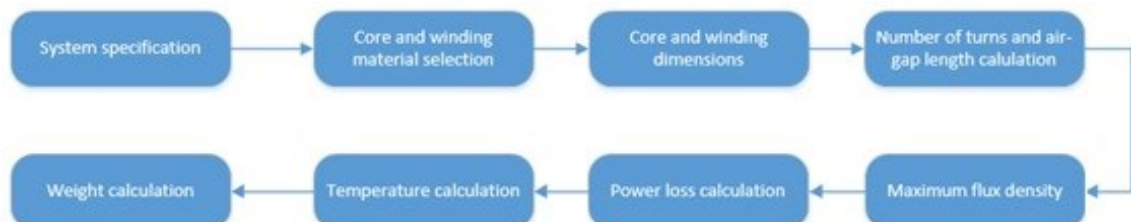


Figure 20 Flowchart of a choke design process. Requirements set by specifications and constraints must be met at every step. Multiple iterations through the flowchart will be needed.

4.2.2 Optimization with Matlab

A Matlab script is used to optimize the designs. A function called “Calculate losses” is created. Nominal current, wire cross-sectional area, wire material and wire total length are given as parameters and the function will return winding resistance, power losses and weight. The function is presented in Algorithm 1.

```
% Calculate losses function
% Returns resistance, power loss and weight of windings. Wire area,
% length, material and nominal current are given as parameters.

function [loss,weight,res] = calculate_losses(area,length,copper,I_RMS)
    Cu_resistivity = 1.68e-8;      % Resistivity at room temp Ohm*m
    Cu_density = 8.96;           % Density g/cm3
    Cu_temp = 3.8e-3;           % Temperature coefficient 1/C
    Al_resistivity = 2.82e-8;    % Resistivity at room temp Ohm*m
    Al_density = 2.7;           % Density g/cm3
    Al_temp = 3.8e-3;           % Temperature coefficient 1/C

    if copper == 1
        R = Cu_resistivity*length/(area/10^6);
        R_high = R*(1+Cu_temp *(120-20));
        W = Cu_density*((area/100)*(length*100));
        W_total = W*2;
        P_loss_winding = I_RMS^2*R_high;
        P_loss_total = 2*P_loss_winding;
    else
        R = Al_resistivity*length/(area/10^6);
        R_high = R*(1+Al_temp *(120-20));
        W = Al_density*((area/100)*(length*100));
        W_total = W*2;
        P_loss_winding = I_RMS^2*R_high;
        P_loss_total = 2*P_loss_winding;
    end

    fprintf('\nResistance in room temperature: %.3f mOhm\n',R*1000);
    fprintf('Resistance in high temperature: %.3f mOhm\n',R_high*1000);
    fprintf('Coil weight of one choke: %.3f kg\n',W/1000);
    fprintf('Coil weight of two chokes: %.3f kg\n',W_total/1000);
    fprintf('Winding loss of one choke: %.3f W\n',P_loss_winding);
    fprintf('Winding loss of two chokes: %.3f W\n',P_loss_total);
    loss = P_loss_winding;
    weight = W;
    res = R;
end
```

Algorithm 1 “Calculate losses” function returns the resistance, power losses and the weight of the winding. Nominal current, winding cross-sectional area, length and material are given as parameters.

This function can be used to calculate resistance, power losses and weight of any winding with known length and area. Depending on given parameter, the function uses values for copper or aluminium. Resistance is calculated and scaled to a high temperature. Losses are calculated based on the scaled resistance and the nominal current. Weight of the winding is calculated based on the volume and density of the material.

Created function returns the value that needs to be optimized. A method for finding the lowest possible value still needs to be established. Design could be done by number of iterations following steps that are presented in Figure 20. Going through a number of iterations can be a lengthy task.

Visual optimization is a useful method for understanding how different parameters affect the outcome. It can be done for example by plotting both the resistance of the winding and saturation flux density as functions of a variable that is being changed. This way a proper value can be chosen for the variable that results in the lowest possible resistivity at an acceptable maximum flux density. An example is presented in Figure 21, where the width of the leg is changed while number of turns are kept constant.

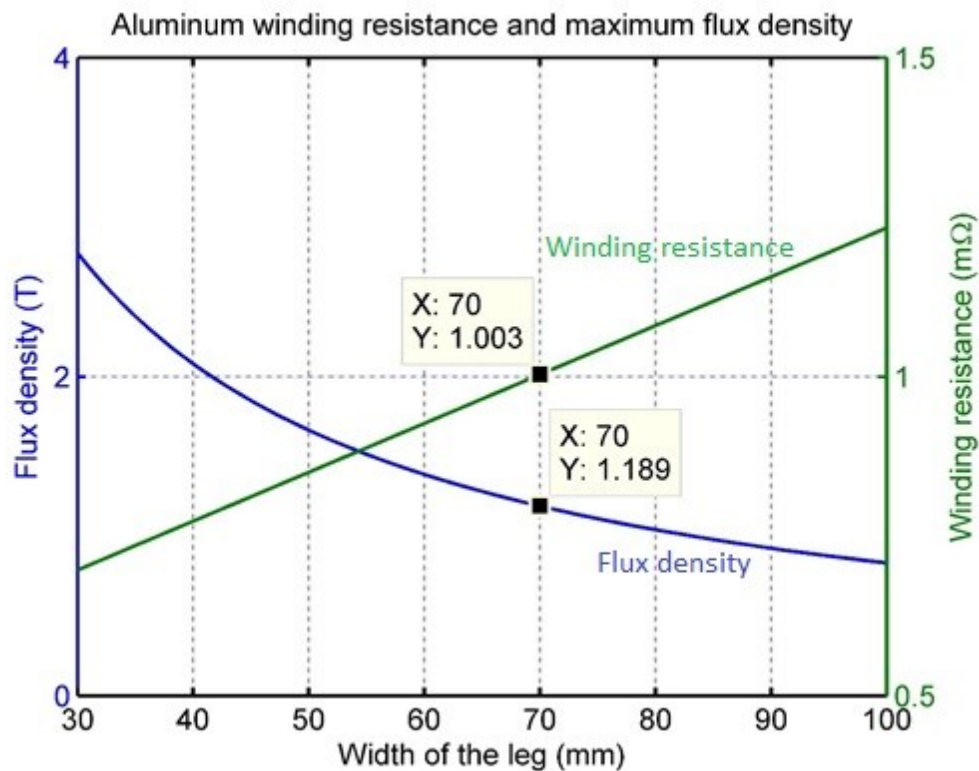


Figure 21 Visual optimization. Width of the leg is increased to find the lowest possible winding losses at an acceptable flux density level.

For an exact answer a system of equations could be put together and solved for power losses. Minimizing the solution would yield the point with smallest losses. A more straightforward method is to use multiple for-loops. This way numerous possibilities and options can be calculated quickly.

This method returns a lot of data and the results can be hard to read in Matlab environment. Data can be easily exported to Excel. Using Excel the data can be sorted for the smallest resistance while adding boundary conditions that filter results that are not acceptable. It is also possible to sort the data for secondary objectives like winding and core weight. An example is presented in Figure 22.

	Centre leg width (mm)	Side leg width (mm)	Stack height (mm)	Choke length (mm)	Choke width (mm)	Wire width (mm)	Wire thickness (mm)	Resistance (mΩ)	Winding weight (kg)	Core weight (kg)	Total weight (kg)	Flux density (T)	Inductance (μH)	Number of turns	Air gap length (mm)	
1																
2		70	35	50	150	196	13	6	0,954	0,556	9,811	10,367	0,76	62,71	10	7,5
3		73	36,5	48	153	202	13	6	0,962	0,560	9,988	10,548	0,76	62,83	10	7,5
4		72	36	49	152	200	13	6	0,962	0,560	10,001	10,561	0,76	63,24	10	7,5
5		71	35,5	50	151	198	13	6	0,962	0,560	10,007	10,567	0,75	62,77	10	7,6
6		73	36,5	49	153	202	13	6	0,969	0,564	10,196	10,760	0,75	63,27	10	7,6
7		72	36	50	152	200	13	6	0,969	0,564	10,205	10,769	0,74	63,26	10	7,6
8		66	33	50	149	188	13	6	0,972	0,566	9,198	9,764	0,76	62,17	10,5	7,9
9		73	36,5	50	153	202	13	6	0,976	0,569	10,404	10,973	0,74	63,95	10	7,6
10		69	34,5	48	152	194	13	6	0,979	0,571	9,388	9,959	0,76	62,43	10,5	7,9
11		68	34	49	151	192	13	6	0,979	0,571	9,393	9,963	0,76	62,79	10,5	7,9
12		67	33,5	50	150	190	13	6	0,979	0,571	9,391	9,961	0,75	62,30	10,5	8,0
13		70	35	48	153	196	13	6	0,987	0,575	9,577	10,152	0,75	62,52	10,5	8,0
14		69	34,5	49	152	194	13	6	0,987	0,575	9,584	10,159	0,75	62,89	10,5	8,0
15		68	34	50	151	192	13	6	0,987	0,575	9,584	10,159	0,74	62,87	10,5	8,0
16		63	31,5	50	149	182	13	6	0,994	0,579	8,780	9,359	0,76	62,21	11	8,3
17		70	35	49	153	196	13	6	0,995	0,579	9,777	10,356	0,75	63,44	10,5	8,0
18		69	34,5	50	152	194	13	6	0,995	0,579	9,780	10,359	0,74	63,63	10,5	8,0
19		67	33,5	47	153	190	13	6	1,002	0,584	8,976	9,560	0,76	62,24	11	8,3
20		66	33	48	152	188	13	6	1,002	0,584	8,980	9,564	0,76	62,60	11	8,3
21		65	32,5	49	151	186	13	6	1,002	0,584	8,978	9,562	0,76	62,91	11	8,3
22		64	32	50	150	184	13	6	1,002	0,584	8,970	9,554	0,75	62,43	11	8,4
23		67	33,5	48	153	190	13	6	1,010	0,588	9,167	9,755	0,75	62,78	11	8,4
24		66	33	49	152	188	13	6	1,010	0,588	9,167	9,756	0,75	63,11	11	8,4
25		65	32,5	50	151	186	13	6	1,010	0,588	9,161	9,750	0,75	63,09	11	8,4
26		74	37	50	151	202	12	6	1,012	0,502	10,372	10,874	0,73	60,99	9,5	7,3
27		60	30	50	149	176	13	6	1,014	0,591	8,362	8,953	0,76	62,09	11,5	8,7
28		67	33,5	49	153	190	13	6	1,018	0,593	9,358	9,951	0,75	63,74	11	8,4
29		64	32	47	153	184	13	6	1,023	0,596	8,574	9,170	0,76	62,22	11,5	8,7
30		63	31,5	48	152	182	13	6	1,023	0,596	8,572	9,168	0,76	62,53	11,5	8,7

Figure 22 Excel spreadsheet that has been sorted for the smallest resistance.

Figure 22 goes to show that basically the same amount of losses can be achieved with multiple different dimensions. Most suitable dimensions can be chosen for further examination. Pseudocode for a loop with three variables is shown in Algorithm 2. The actual code used in the design process is given in appendix A.

```

for a = range_a
  for b = range_b
    for n_turns = range_turns
      calculate_area
      calculate wire length
      calculate air gap
      calculate flux density
      calculate losses
      calculate weight
    end
  end
end
end

```

Algorithm 2 Pseudocode for the optimization script.

Ranges for the variables have to be determined and filters can be added already at this point. The script needs to be rewritten for different core shapes but it is only a matter of geometry. The main idea of the algorithm is the same independent of the core shape.

After choosing the most intriguing options from the spreadsheet, AutoCAD is used to visualize the available room and space taken by these different solutions. Cable connections, mounting brackets and other extruding pieces need to fit inside the required area as well. Numbers can look good on paper, but it is necessary to check that the design is feasible.

Finally the design is modelled in Maxwell to check that the flux density in the core stays below saturation levels. Maxwell can also be used to evaluate inductance of the design. If the magnetic model is built to be parametric, optimization can be done by Maxwell as well. However, if the range of the variables is large, simulation can take a long time. For this reason the initial optimization is performed with the Matlab script.

5. NEW DESIGNS AND PROTOTYPES

This section presents the new designs and their prototypes. Measurement results and comparison to the reference chokes are also given. Manufacturability and cost of the prototype chokes are evaluated and compared to the reference chokes.

5.1 INTRODUCTION OF NEW DESIGNS AND PROTOTYPES

Three different DC-choke prototypes are presented in this section. Core material is kept the same for all of the designs in order to put emphasis on the winding techniques and core shapes. Magnetic model and flux density simulation are presented for each design. Comparison to the original DC-choke is performed for every design.

5.1.1 Design A

This prototype is a shell type DC-choke. Two chokes are required for the operation of the frequency converter. Basic information about the choke is shown in Table 10.

Table 10 Design A basic information.

Number of turns	9
Winding material	Aluminium
Winding method	Vertically wound
Wire size	13,5x6 mm rectangular wire
Core material	Non-oriented magnetic steel M470-50A
Core area	3430 mm ² / 1862 mm ²

13,5x6 mm vertically wound aluminium wire is used for the design. The core area of the centre leg is twice the area of the side legs. Due to large core area, the required inductance can be achieved with only 9 turns. Dimensions of the choke and the magnetic model created with Ansys Maxwell is presented in Figure 23.

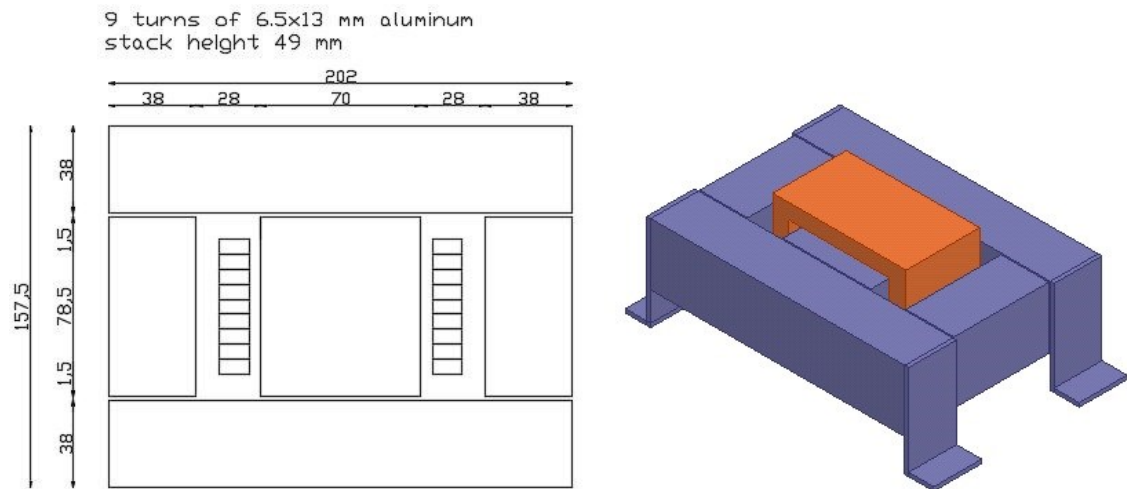


Figure 23 Dimensions and magnetic model of design A.

The height of the stack is 49 mm, the total width of the choke is 157,5 mm and the total length of the choke is 202 mm. The centre leg of the choke is wider than the side legs. Full amount of flux is flowing through the centre leg and then it is distributed evenly to both side legs. The side legs and top and bottom yokes can be manufactured from strips that have half the width of the centre leg without driving the core to saturation. Flux density distribution is calculated using Maxwell. Flux density at nominal current and saturation current is presented in Figure 24.

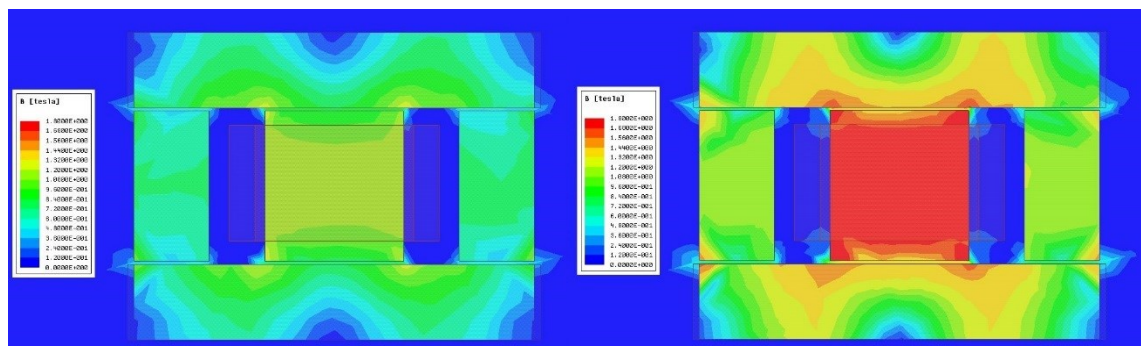


Figure 24 Flux density distribution at 423A and at 700A. Scale runs from 0 to 1,8 T

Air gaps are added to both ends of every leg. Total air gap of the core equals two times the airgap in the centre leg. Air gaps should be divided into multiple smaller gaps but in order to simplify the prototype manufacturing gaps at both ends of the legs are used.

Vertical winding is used to fit the windings into a smaller space. Length of the choke will decrease and the saved material can be used to increase the cross sectional area of the core. Larger cross-sectional area allows smaller number of turns which decreases the resistance of the coil. Aluminium winding up to 13mm x 6.5mm can be wound vertically. With larger wire sizes the enamelled surface of the wire can't take the stress and starts to tear. Also the amount of force needed increases and the fiberglass spacers break under the pressure. This means that a separate coil former would need to be used.

Table 11 Comparison between the reference DC choke and design A.

	Reference DC Choke	Design A	Difference (%)
Height (mm)	93	93	0 %
Width (mm)	135	154,5	14 %
Length (mm)	280	202	-28 %
Winding mass Cu (kg)	2,516	-	-
Winding mass Al (kg)	-	0,538	-79 %
Mass of core (kg)	7,68	10,34	35 %
Total mass (kg)	10,198	10,878	7 %
Resistance (m Ω)	1,332	0,758	-43 %

Tensile strength of copper is larger than that of aluminium, so copper rectangular wire would need to be a couple of millimetres narrower if it were to be used without a separate coil former. The resistance of the copper coil at these dimensions is only slightly smaller than the resistance of the aluminium coil. Aluminium is chosen due to cheaper price and easier winding process.

Comparison between the original DC-choke and calculated values for design A is presented in Table 11. It can be seen from the table that winding mass is substantially reduced while the core mass is increased. This is a beneficial trade as copper is expensive and magnetic steel is rather cheap. Total mass of the choke is only slightly increased. Winding resistance is decreased by 43 %. This achieved by decreased number of turns and increased wire size. The prototype of the design was manufactured by Trafotek. Picture of the prototype is presented in Figure 25.

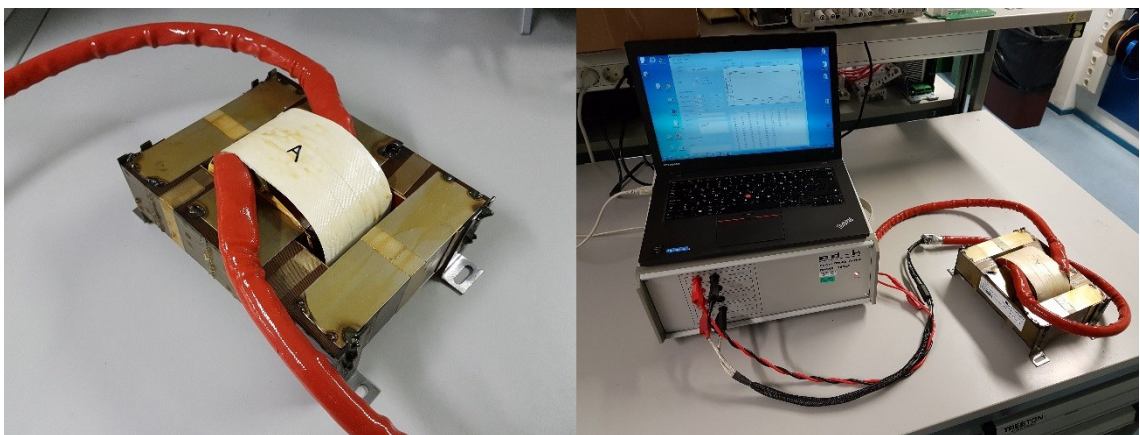


Figure 25 Prototype of design A. The coil of the choke is made of vertically wound rectangular aluminium wire.

During prototype process it became clear that 9 turns of aluminium wire couldn't be fit into the winding window due to productional reasons. Number of turns was cut down by one in order to successfully manufacture the prototype. This meant that the air gaps needed to be reduced in order to obtain the correct inductance. Smaller air gaps reduced the saturation current of the prototype slightly below the initial design point. This could have been worked around by making changes to the dimensions of the core, but due to tight schedule the prototype was manufactured as is.

5.1.2 Design B

This prototype is a core type choke that has both the + and - windings around the same core. Only one choke is needed to operate the frequency converter. The same flux is passing through both windings. A centre leg is not necessarily needed but it can be used for suppression of common mode currents. Without the centre leg the flux created by common mode currents would not have a low reluctance path to flow in. The centre leg also helps in the case of an earth fault. In this case all the current would pass through only one winding and the flux created by the operating choke would cause voltage rise in the non-operational winding. However with the centre leg in place, flux passes through the centre leg and no voltage is induced into the non-operational coil. Basic information for design B is given in Table 12.

Table 12 Design B basic information.

Number of turns	10,5
Winding material	Aluminium
Winding method	Foil wound
Wire size	120x1 mm foil
Core material	Non-oriented magnetic steel M470-50A
Core area	3430 mm ²

Having both windings around a common core allows a larger core area and winding window. At this point aluminium foil is by far the best option. Copper foil could be used as well. However, according to choke manufacturers, copper foil is so scarcely used that the price difference to aluminium foil is even bigger than with wires. Thus aluminium foil is chosen for the prototype. Dimensions and magnetic model of design B are shown in Figure 26.

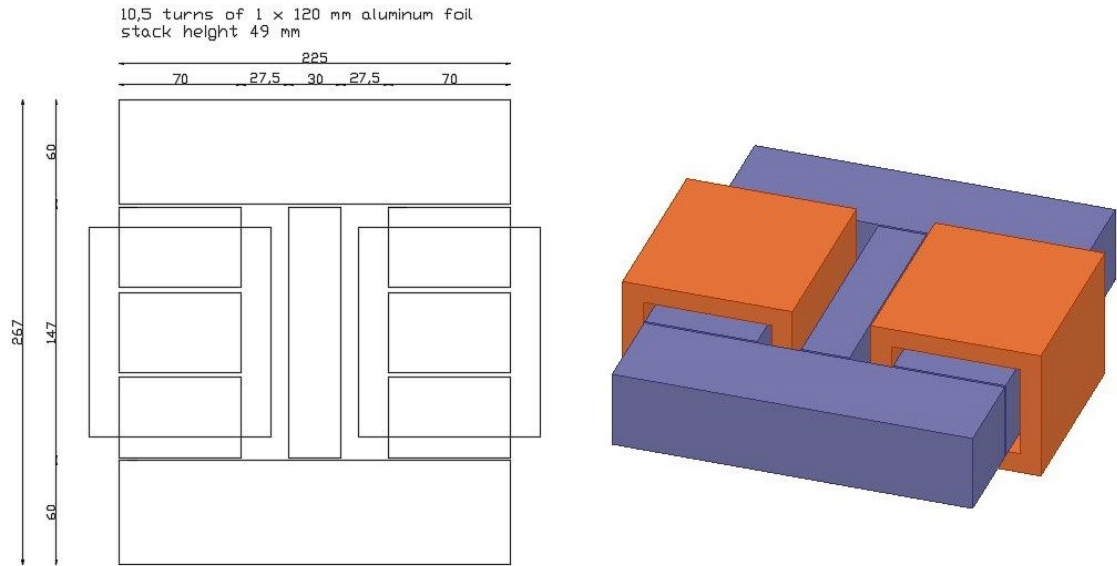


Figure 26 Dimensions and magnetic model of Design B.

Flux is rotating through both windings. Windings share a common return path so this design allows a smaller amount of core material to be used. Flux density distribution and the direction of the flux lines for both differential and common-mode currents are calculated using Maxwell. Flux density at nominal and saturation current is presented in Figure 27.

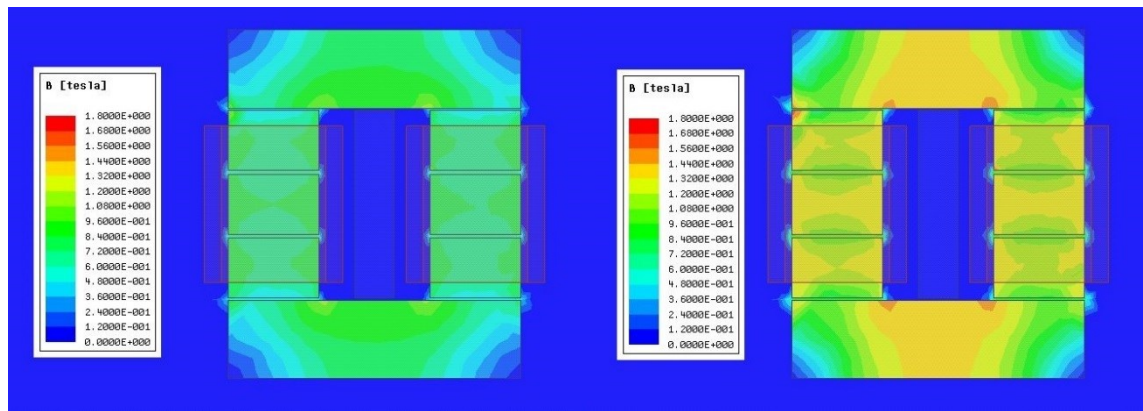


Figure 27 Magnetic flux density distribution at 423 A and 700 A. Scale runs from 0 to 1,8 T.

A small centre leg is added for common-mode currents. It can be seen from Figure 27 that no flux is flowing in the centre leg. If the direction of the current in one of the legs is changed, magnetic flux starts to flow in the centre leg as well. If the centre leg was missing, the flux created by common-mode currents would not have a low reluctance path and common-mode inductance would be low. Simulated behaviour of flux lines with differential and common-mode excitations are presented in Figure 28.

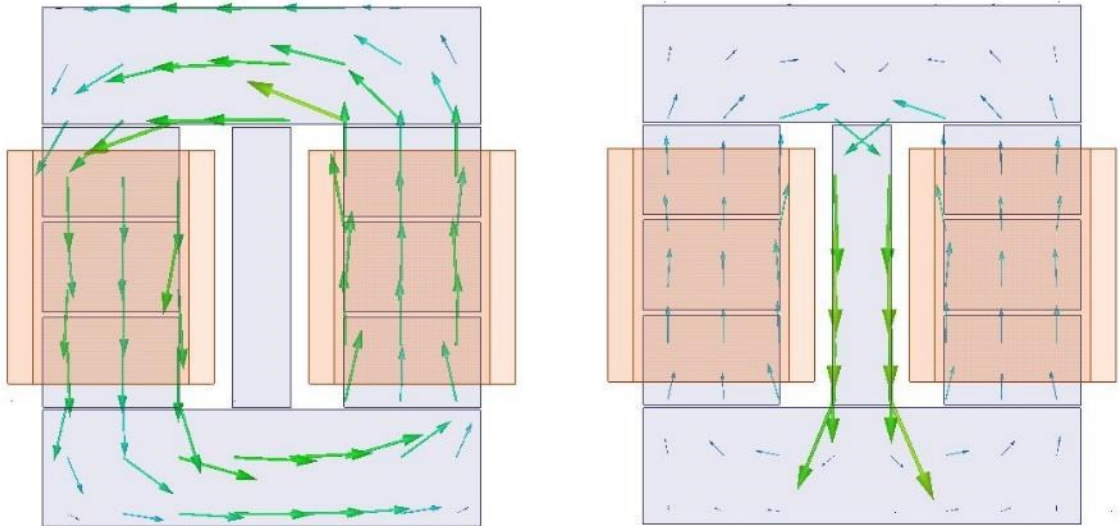


Figure 28 Magnetic flux behaviour with differential and common mode current. Common mode flux lines have been scaled up for better illustration.

Common-mode currents are small compared to the differential current. This means that the common-mode flux is also small. Flux lines in the common-mode figure have been scaled up for better demonstration. Centre leg of the core could be even smaller as the flux density created by the common mode currents won't drive the leg to saturation. Comparison between the reference DC-choke and design B is presented in Table 13.

Table 13 Comparison between the reference DC-choke and design B. Winding mass and resistance is presented for one coil. Dimensions and mass of the choke is divided by two.

	Original DC Choke	Design B	Difference (%)
Height (mm)	93	93	0 %
Width (mm)	135	154,5	14 %
Length (mm)	280	267	-4,6 %
Winding mass Cu (kg)	2,516	-	-
Winding mass Al (kg)	-	0,868	-65 %
Mass of core (kg)	7,68	8,28	7,8 %
Total mass (kg)	10,198	9,148	-10,3 %
Resistance (mΩ)	1,332	0,906	-32 %

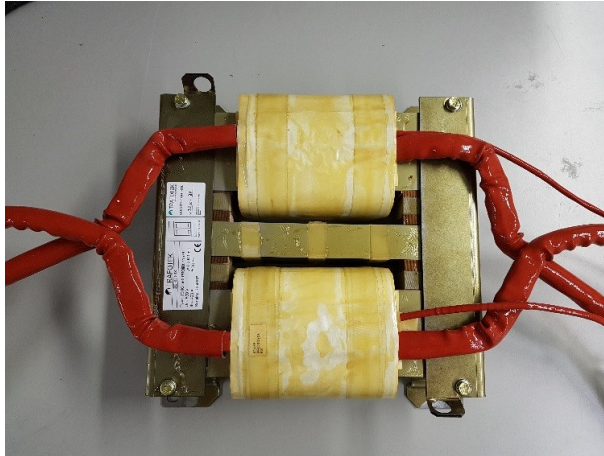


Figure 29 Prototype of design B. The coil of the choke has been made of aluminium foil. There is no windings on the center leg.

Resistance of the prototype is 32 % smaller than the resistance of the original DC-choke. Mass of the core is only slightly increased. Winding mass is substantially reduced which means that the total mass of the choke is reduced by 10,3 %. Prototype for design B is also manufactured by Trafotek. This design is cheap and easily manufactured as it uses aluminium foil windings. Picture of the prototype is show in Figure 29.

5.1.3 Design C

Due to the confidential nature of design C, it is presented in more detail in confidential appendix B. This choke was designed to be a DC-choke but it could be used as an AC-choke as well. The idea of the design is to utilize the winding window as well as possible by utilizing a new type of winding method and unconventional core shape. The design aims for a high power density. This prototype is assembled by hand at ABB laboratory. Comparison to original DC choke is presented in Table 14.

Table 14 Comparison between the reference DC-choke and design C.

	Reference DC-choke	Design C	Difference (%)
Height (mm)	93	91,5	-2 %
Width (mm)	135	160	19 %
Length (mm)	280	160	-34 %
Winding mass Cu (kg)	2,516	2,801	11%
Mass of core (kg)	7,68	9,376	22 %
Total mass (kg)	10,198	12,177	19 %
Resistance (mΩ)	1,332	0,3980	-70 %

The efficiency of the design can be seen from the values. The amount of copper is only slightly increased by 11%, yet the resistance of the design is 70% smaller than the resistance of the reference DC-choke. If aluminium was used the winding mass would be lower and the losses would still be 50% smaller. Width of the choke is increased by 17 % while the length of the choke is decreased by 34 %. Overall outer dimensions of the choke are actually reduced but the mass of the core is increased by 22 %. A bigger cross-sectional area can be fitted in to a smaller space due to the unconventional core shape and winding method of the choke.

5.2 TEST RESULTS

Inductance, resistance and thermal measurements are carried out with the prototypes in order to verify the calculated values. The results of the measurements will be compared to the results of the measurements performed on the original DC-choke and to the values calculated during design process. Reasons for anomalies will be evaluated and improvements are suggested for the prototypes.

5.2.1 Inductance measurement

Inductance of the prototype chokes were measured with pulse tester. Inductance of the chokes are plotted against current in Figure 30. Nominal inductance is 64 μH and it is shown in the figure as a solid red line. A tolerance of $\pm 10\%$ is plotted on the chart with a dashed red line. Target saturation current is 700 A. The inductance of the choke should stay within the tolerance in order to fulfil the specification for the choke.

Prototype A follows the inductance curve of the original DC choke up until 600 A. From here on the curve of prototype A turns in to a bit steeper decline than the curve of the reference choke, crossing the -10 % line just before 700 A. The smaller saturation current is due to bit higher flux density than was planned. Initial design was for 9 turns, but only 8 turns could be fitted due to manufacturing reasons. Air gaps of the core had to be made a bit smaller in order to achieve proper inductance. Smaller airgaps reduce the reluctance of the circuit and increase flux density.

Inductance of prototype B is around 68 μH , which is a bit higher than the inductance of the original DC-choke. Saturation current of the choke is also higher. Combining the two cores into one allowed a more room for the choke. The core could be designed without as many restrictions as with two cores. Measured common-mode inductance of the choke was around 30 μH .

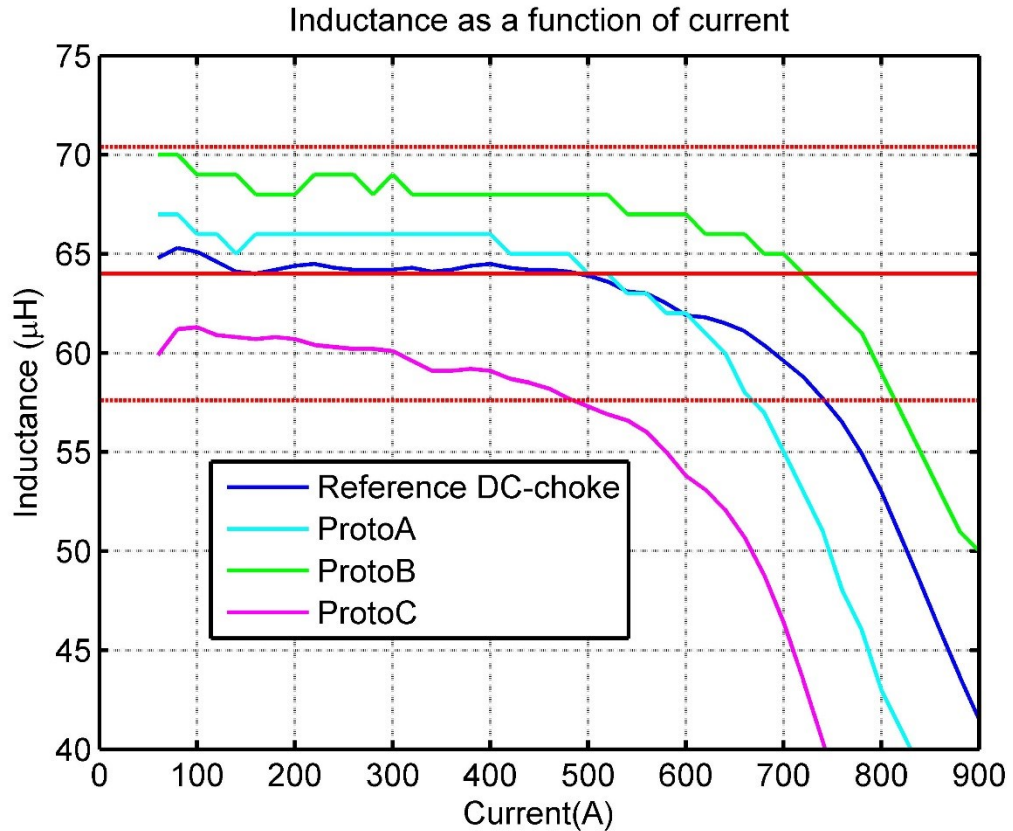


Figure 30 Inductance curves of the reference DC-choke and the prototypes.

It is apparent that the inductance of prototype C is a bit low. The inductance of the choke starts at 62 μH , and the core starts to saturate at less than 600 A. The core area of the choke or the number of turns needs to be increased slightly in order to obtain the specified inductance. Reasons for these anomalies are discussed in confidential appendix B.

5.2.2 Resistance measurement

Calculated resistances of the new designs are smaller than the resistance of the reference DC-choke. Measured resistances in room temperature are presented in Table 15.

Table 15 Resistance of the chokes at room temperature.

	Micro-ohm meter	Current source and voltage measurement
Reference DC-choke	1,370 m Ω	1,366 m Ω
Prototype A	0,850 m Ω	0,845 m Ω
Prototype B	0,847 m Ω	0,841 m Ω
Prototype C	0,488 m Ω	0,486 m Ω

Prototype C has clearly the smallest resistance of the chokes. However it is worth noting that inductance of the choke was lower than the inductance of the other chokes. The cross-sectional area or the number of turns need to be increased in order to achieve proper inductance. This is bound to slightly increase the resistance of the winding. Prototypes A and B have roughly 38% smaller losses than the original DC-choke while resistance of prototype C is almost 65% smaller.

5.2.3 Thermal behaviour

Resistance measurements were done at room temperature. Power losses that occur in the windings of the chokes is dissipated as heat. Increased temperature increases the resistance of the coil. Total heating power and the ability to dissipate the heat determines how high the temperature rises.

Chokes are installed in to the frame of the frequency converter and measuring clips are attached to the ends of the windings. Thermocouples are placed in the predicted hotspots. Nominal current 423 A is passed through the chokes. Resistance of the windings can be calculated based on the current and measured voltage. The frequency converter has forced ventilation produced by two fans. Resistances of the chokes are presented in Figure 31.

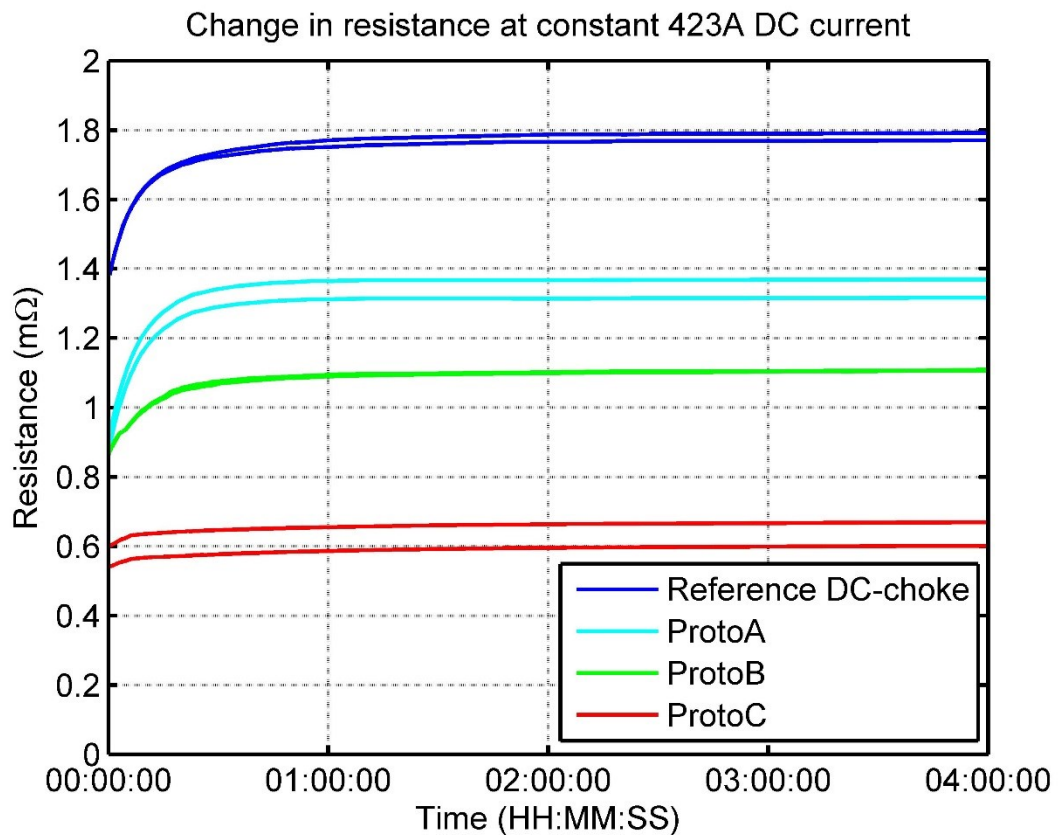


Figure 31 Change in resistance of the windings at nominal current. Increase in resistance is proportional to the temperature rise. Resistance is presented for both the + and – chokes. The resistance of prototype B’s windings are almost identical.

Resistance of the reference DC-choke is still the largest. After reaching thermal equilibrium resistance of the choke is increased by 31 % to 1,8 m Ω .

Prototype A had 38 % smaller resistance in room temperature than the reference DC-choke. However after reaching thermal equilibrium the resistance is substantially increased by 53 % to 1,3 m Ω . The difference compared to the reference DC-choke is only 30 %. The prototype is operating at a much higher temperature than the reference DC-choke.

In room temperature the resistance of prototype B was practically the same as the resistance of prototype A. However under nominal current the resistance of prototype A is higher. The resistance of prototype B is increased by 30 % to 1,1 m Ω . Resistance under nominal current is still 39 % smaller than the resistance of the reference DC-choke.

Resistance of prototype C is still the smallest of the chokes. It can be seen that the temperature of the choke stays low. Power losses of the windings are so small that the created heat can easily be dissipated. At thermal equilibrium the resistance of prototype C is 66% smaller than the resistance of the original choke.

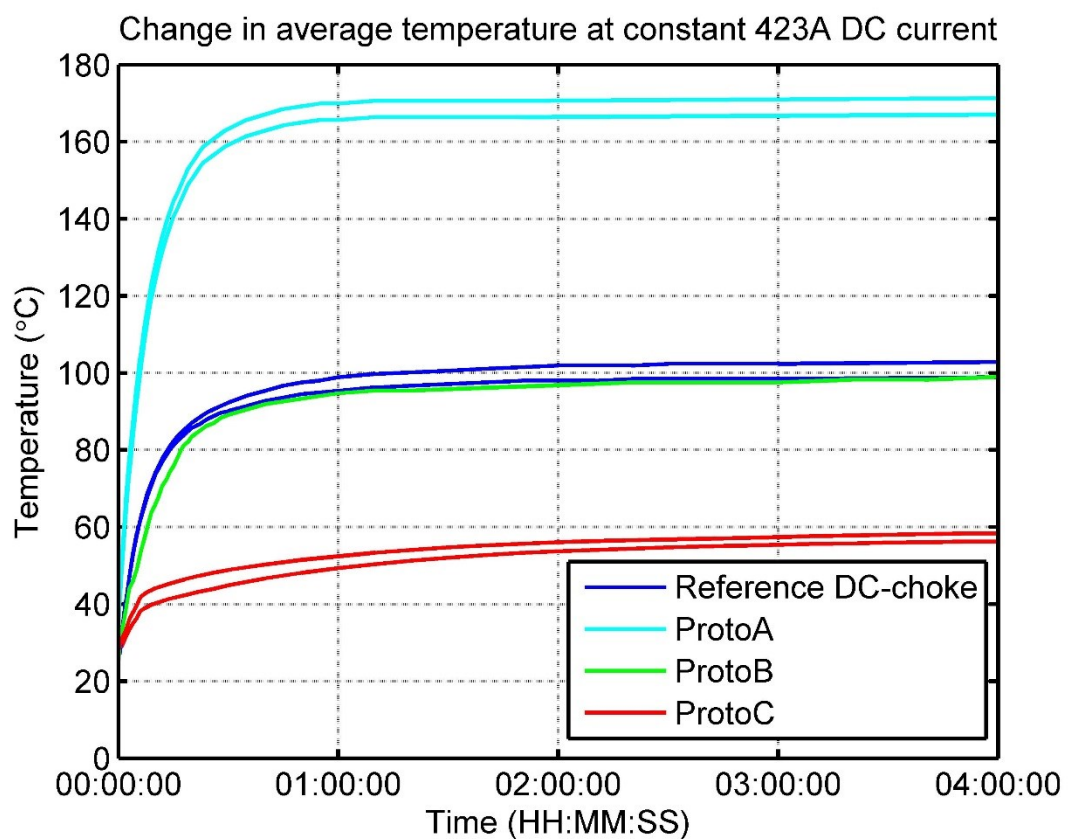


Figure 32 Average temperature of the windings at nominal current. Temperatures are calculated based on the changing resistance.

Average temperature of the windings can be calculated based on the changes in resistance according to (48) presented on page 32. Changing average temperature of the windings is presented in Figure 32.

Temperature of prototype A is way above the other chokes. For this reason the resistance of the choke increased the most in Figure 31. Prototype A heats up to over 160 degrees. Heat dissipating surface area of the choke is too small to dissipate the heat. The EI shape of the core is not ideal for cooling as convection doesn't reach all sides of the coil. The reference DC-choke reaches thermal equilibrium at around 100 degrees. Thermal behaviour of prototype B is almost identical to the reference DC-choke.

Winding temperature of prototype C is only 60 degrees. Windings of the choke allow a big area for heat dissipation and generated heat is small. Volume of the core material is largest in this design and it takes longer for the prototype to reach thermal equilibrium compared to the others.

Thermocouples were placed at predicted hotspots of each choke. For the reference DC-choke and prototypes A & B, this is between the core and the winding. For prototype C the predicted hot spot is between two turns of winding. Measured temperatures are shown in Figure 33.

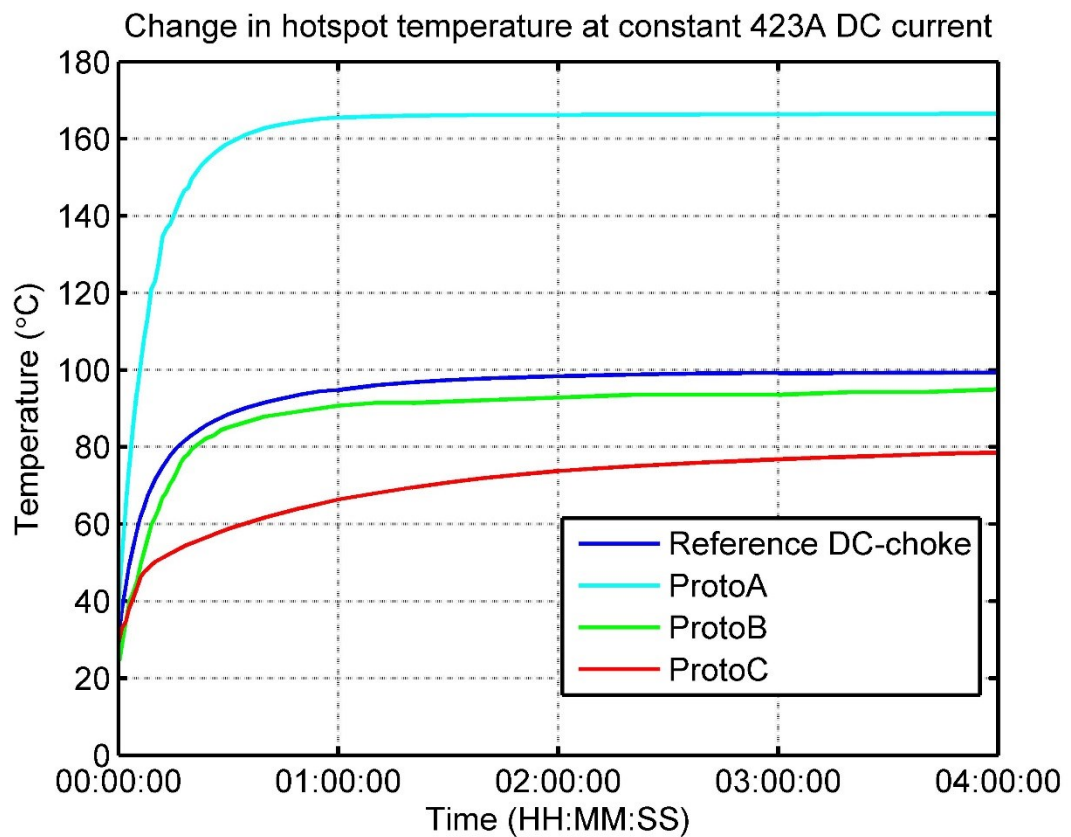


Figure 33 Measured temperatures at predicted hotspots at nominal current.

The measured temperatures of the reference DC choke, prototype A and prototype B are really close to the average temperatures calculated based on the resistance change. Temperature at the hotspot of prototype C is around 80 degrees, which is 20 degrees higher than the average temperature.

5.3 COST ESTIMATE AND MANUFACTURABILITY

Cost of the choke consist of material and labour costs. Material costs are pretty straightforward to compare, but labour costs are a lot harder to evaluate. Cost caused by the power losses can also be calculated, but it is more in the interest of the customer. A comparison of aspects affecting the cost of the choke is presented in Table 16.

Material cost can be further divided into core and winding cost. All of the prototype chokes have the same core material which allows a simple comparison through core masses. Total core mass is lowest in prototype B which has both the plus and minus windings on the same core. Core of the reference DC-choke is the second lightest. Core of prototype C has a larger mass than the reference DC-choke. Prototype A has the biggest core mass of the prototypes but the AC-choke variant has by far the biggest core mass of all the chokes. However the cost of the core material is low, so the difference in core prices are not remarkable.

The reference DC-choke and prototype C have copper windings while rest of the chokes have aluminium windings. Material prices are fluctuating based on the commodity markets. At the time of writing the thesis the price of copper was three times the price of aluminium. Prototype C has the highest winding mass of the chokes, but the difference to the reference DC-choke is only 0,3 kg. The winding material of the reference AC-choke is aluminium, but the total weight of the windings is still over 3 kg. DC-chokes generally require less winding material as they have only two windings compared to three of the AC-chokes.

Table 16 Cost comparison between different designs. The masses include two chokes for the reference DC-choke and prototypes A and C.

	Core mass (kg)	Winding mass (kg)		Manufacturing cost
		Al	Cu	
Original DC-choke	15,360		5,032	Medium
Original AC-choke	25,324	3,124		Low
Proto A	20,680	1,760		Medium
Proto B	16,560	1,736		Low
Proto C	18,752		5,602	Medium/High

Amount of labour needed for different winding methods needs to be also taken into account. Traditional chokes are cheaper to produce because sub-contractors are more likely to have the machinery and experience to manufacture them. According to the manufacturer aluminium foil is the simplest of the presented options. Winding on the original DC choke is also straightforward, but not as fast as aluminium foil. It requires more manual labour. Vertical winding is also automated but the lack of capable machinery would require investments.

Prototype C has a completely new winding method which means that the manufacturing process needs to be thought up from the scratch. At the moment the choke is the most expensive of the presented options. The manufacturing cost of the choke is hard to evaluate without further research and development. The modular structure of the choke could allow multiple different suppliers which in turn would yield manufacturing cost savings through competitive tendering.

Manufacturing cost is lowered for the AC-choke variant and prototype B due to the single choke design. Rest of the designs require two separate chokes which increases cost. On the other hand the lighter chokes are much easier to handle during the assembly of the frequency converter. Installing two 10 kg chokes is a lot simpler than one 30 kg choke.

6. CONCLUSIONS

The objective of the thesis was to design a low loss and cost-efficient choke for a general purpose frequency converter utilizing different winding methods and core shapes. Power losses need to be lowered while still meeting magnetic, thermal and size requirements. A balance needs to be found between cost of the choke and the allowed power loss level. Decreasing the power losses beyond a certain point becomes extremely expensive and impractical.

Design of a cost-efficient and low loss choke is a complex process with multiple stages. Increasing the efficiency of the choke can prove to be difficult if conventional methods are used. Sticking to the conventional core shapes and winding methods means that there is only a limited amount of possibilities to affect the outcome.

Choke design is usually done under strict size restrictions based on the mechanical point of view. These restrictions can force the design process into a certain direction and discard some otherwise viable options. If the dimension constraints could be ignored and the choke could be freely optimized, the ideal choke would resemble a square rather than a rectangle.

For example in a standard core type choke, increasing the length of the leg doesn't add to the magnetic performance of the choke. Increasing the width of the leg or the height of the stack contributes to inductance. Length of the leg should only be increased if sufficient cooling is not otherwise achieved.

Three different choke designs were introduced in the thesis. The first prototype is a shell type inductor that has a coil made of vertically wound rectangular aluminium wire. The second prototype is a core type inductor that has both the + and – coils around the same core. The coils are wound with aluminium foil. An extra leg is added in the centre of the choke for common mode flux. The third prototype utilizes a novel winding method and unconventional core shape.

Compromises need to be done during the designs process. It is not possible to achieve a design that excels in every aspect. The objectives and priorities of the design process need to be clear. Positive and negative aspects of each design is given in Table 17.

Table 17 Positive and negative aspects of each design.

Design	Positive	Negative
Reference DC-choke	Low manufacturing cost Efficient cooling Small size	High losses Material cost (~5kg of Cu)
Reference AC-choke	38 % lower resistance Low manufacturing cost Efficient cooling	Material cost (~3,1kg of Al) Large core mass and size
Prototype A	30% lower resistance Simple core manufacturing Low material cost	Winding technique sets constraints on wire dimensions. Poor cooling
Prototype B	39% lower resistance Low manufacturing cost Small size	Requires changes in the wiring layout of the converter.
Prototype C	66% lower resistance Small size Efficient cooling	Complicated to manufacture Material cost (~5,6kg of Cu)

Prototype A revealed the downsides of vertically wound wire. With wire wound into such a tight package, the surface area dissipating the heat is reduced substantially. Initially moderately low resistance is increased due to high temperature. The wires could be wound with more slack, but it would diminish the advantages of vertical winding.

Power losses of prototype B are reduced moderately and the core and coil weight are both slightly reduced. Manufacturing of the choke is straightforward and the coil material is not expensive. The frequency converter is designed for two individual chokes instead of one, so using design B would require changes in the cable routing.

Prototype C is an intriguing design. The resistance of the windings is 66 % smaller at nominal current while the amount of copper is increased by only 11 % compared to the reference choke. Small power losses and large winding surface area keep the temperature of the choke low. The width of the choke is increased slightly while the length is decreased. On the downside, the choke is more expensive to manufacture than the reference choke.

Further research is proposed on design C. The created prototype is feasible, but it is not suited for industrial manufacturing. The design should be reworked from manufacturing point of view. The margin between the resistances of prototype C and the reference DC-choke is so large that there is plenty of room for adjustments that make the manufacturing process easier. Material cost could be cut down by using aluminium windings while still maintaining a substantial decrease in power losses. Aluminium prototype should be manufactured and tested.

Objectives of the thesis have been achieved by means of the three prototypes. Different winding methods and core shapes were utilized in the choke design. Resistance of the windings was successfully reduced in all designs. Measurements performed on the chokes revealed the positive and negative aspects of different design concepts. These aspects should be taken into account for the next round of prototypes.

REFERENCES

- [1] J. W. Kolar, J. Biela, S. Waffler, T. Friedli, U. Badstuebner, Performance trends and limitations of power electronic systems, 2010 6th International Conference on Integrated Power Electronics Systems, pp. 1-20.
- [2] F. Zare, H. Soltani, D. Kumar, P. Davari, H. A. M. Delpino, F. Blaabjerg, Harmonic Emissions of Three-Phase Diode Rectifiers in Distribution Networks, IEEE Access, Vol. 5, 2017, pp. 2819-2833.
- [3] W. G. da Silva, M. A. A. de Freitas, I. Kopcak, IEEE Standard 519-92 and the harmonic currents caused by the inverter fed induction motor, 2013 Brazilian Power Electronics Conference, pp. 1283-1290.
- [4] D. E. Rice, A detailed analysis of six-pulse converter harmonic currents, [1992] Record of Conference Papers Industry Applications Society 39th Annual Petroleum and Chemical Industry Conference, pp. 153-163.
- [5] IEEE Standard Definitions for the Measurement of Electric Power Quantities Under Sinusoidal, Nonsinusoidal, Balanced, or Unbalanced Conditions, in: IEEE Std 1459-2010 (Revision of IEEE Std 1459-2000), 2010, pp. 1-50.
- [6] Y. Yang, K. Zhou, H. Wang, F. Blaabjerg, Harmonics mitigation of dead time effects in PWM converters using a repetitive controller, 2015 IEEE Applied Power Electronics Conference and Exposition (APEC), pp. 1479-1486.
- [7] IEEE Recommended Practice and Requirements for Harmonic Control in Electric Power Systems, in: IEEE Std 519-2014 (Revision of IEEE Std 519-1992), 2014, pp. 1-29.
- [8] IEC Adjustable speed electrical power drive systems - Part 3: EMC requirements and specific test methods, in: IEC Std 61800-3-2015, 2015.
- [9] IEC Electromagnetic compatibility of technical equipment. Limitation of emission of harmonic currents in low-voltage power supply systems for equipment with rated current greater than 16 A. Limits and test methods, in: IEC Std 61000-3-4, 2006.
- [10] F. L. Hoadley, Comparison of Methods for the Mitigation of Line Disturbances Due to PWM AC Drives, Conference Record of 2007 Annual Pulp and Paper Industry Technical Conference, pp. 78-92.
- [11] A.Y. Abdelaziz, S.F. Mekhamer, S.M. Ismael, Technical considerations in harmonic mitigation techniques applied to the industrial electrical power systems, 10-13 June 2013, Stockholm.
- [12] K. Lee, T. Jahns, D. W. Novotny, T. A. Lipo, W. E. Berkopec, V. Blasko, Impact of Inductor Placement on the Performance of Adjustable-Speed Drives Under Input

Voltage Unbalance and Sag Conditions, IEEE Transactions on Industry Applications, Vol. 42, Iss. 5, 2006, pp. 1230-1240.

[13] A. R. Strandt, R. M. Tallam, Comprehensive analysis of drive performance when using a dc link choke vs. an input line reactor, 2015 IEEE Energy Conversion Congress and Exposition (ECCE), pp. 2876-2883.

[14] D.A. Fleisch, A student's guide to Maxwell's equations, Cambridge University Press, Cambridge, UK ; New York, 2008, 134 p.

[15] N. Mohan, W.P. Robbins, T.M. Undeland, Power electronics : converters, applications and design, 3rd ed ed. Wiley, Hoboken (NJ), 2003, 802 p.

[16] A. Ayachit, M. K. Kazimierczuk, Sensitivity of effective relative permeability for gapped magnetic cores with fringing effect, IET Circuits, Devices & Systems, Vol. 11, Iss. 3, 2017, pp. 209-215.

[17] R.W. Erickson, D. Maksimovic, Fundamentals of Power Electronics, Springer, Norwell, Massachusetts, 2001.

[18] M.K. Kazimierczuk, High-Frequency Magnetic Components, Wiley, Somerset, GB, 2013.

[19] C.W.T. MacLyman, Transformer and inductor design handbook, 3. ed., rev. and expanded ed. Dekker, New York, 2004.

[20] J. Muhlethaler, J. W. Kolar, A. Ecklebe, A novel approach for 3d air gap reluctance calculations, 8th International Conference on Power Electronics - ECCE Asia, pp. 446-452.

[21] Xi Nan, C. R. Sullivan, Simplified high-accuracy calculation of eddy-current loss in round-wire windings, 2004 IEEE 35th Annual Power Electronics Specialists Conference (IEEE Cat. No.04CH37551), pp. 879 Vol.2.

[22] K. Emori, T. Shimizu, Y. Bizen, Discussion on design optimization of inductor loss focused on copper loss and iron loss, 2013 1st International Future Energy Electronics Conference (IFEEEC), pp. 241-245.

[23] A. Ayachit, M. K. Kazimierczuk, Steinmetz Equation for Gapped Magnetic Cores, IEEE Magnetics Letters, Vol. 7, 2016, pp. 1-4.

[24] A. Dauhajre, R. D. Middlebrook, Modelling and estimation of leakage phenomena in magnetic circuits, 1986 17th Annual IEEE Power Electronics Specialists Conference, pp. 213-226.

[25] A.v.d. Bossche, V. Valchev, Inductors and transformers for power electronics, Taylor & Francis, Boca Raton, 2005, 447 p.

[26] R. Wrobel, N. McNeill, P. H. Mellor, Thermal analysis of a high energy density pre-biased choke, 2008 18th International Conference on Electrical Machines, pp. 1-4.

[27] BS EN 60085:2008: Electrical insulation. Thermal evaluation and designation, British Standards Institute, 2009.

[28] Ingress Protection (IP) According to EN 60529 / DIN 40050, <http://www.moltecin-ternational.com/support/protection.html>.

[29] A. Krings, A. Boglietti, A. Cavagnino, S. Sprague, Soft Magnetic Material Status and Trends in Electric Machines, IEEE Transactions on Industrial Electronics, Vol. 64, Iss. 3, 2017, pp. 2405-2414.

[30] A. Krings, M. Cossale, A. Tenconi, J. Soulard, A. Cavagnino, A. Boglietti, Characteristics comparison and selection guide for magnetic materials used in electrical machines, 2015 IEEE International Electric Machines & Drives Conference (IEMDC), pp. 1152-1157.

[31] A. H. Jahidin, M. S. A. Megat Ali, W. N. L. W. Mahadi, Magnetic properties of grain-oriented and non-oriented silicon iron core arrangements, 2011 IEEE International Conference on System Engineering and Technology, pp. 172-176.

[32] One year price for aluminium and copper, <http://www.infomine.com/investment/metal-prices>.

[33] C. R. Sullivan, Aluminum Windings and Other Strategies for High-Frequency Magnetics Design in an Era of High Copper and Energy Costs, IEEE Transactions on Power Electronics, Vol. 23, Iss. 4, 2008, pp. 2044-2051.

APPENDIX A: AN EXAMPLE OF THE MATLAB SCRIPT USED FOR OPTIMIZATION

```

% New design calculation
clear
clc
I_RMS = 423; % Nomial current
I_peak = 700; % Peak current
L=64e-6; % Inductance
B_max = 1.2; % Maximum flux density
copper = 0; % 0=aluminium, 1=copper
Fe_density = 7.874; % Density of iron
y_0 = pi*4e-7; % Permeability of free space

spacer = 3e-3; % Space left between wire and core
range1 = (30:50)*1e-3; % Range for stack height
range2 = (50:100)*1e-3; % Range for centre leg width
range3 = (10:13.5)*1e-3; % Range for wire width
range4 = (4:6)*1e-3; % Range for wire thickness
n=1; % Initialize pointer

for b = range1
for a1 = range2
for wire_width = range3
for wire_thickness = range4

% Calculate area
a2 = a1/2; % Width of the side leg
A_wire = wire_thickness*wire_width; % Area of the conductor
A_core = a1*b; % Area of the core

%Air gap calculation
w_gap = 0.5*L*I_peak^2; % Energy in the airgap
l_gap = w_gap/(0.5*B_max^2/y_0*A_core); % Length of total airgap
l_gap_single = l_gap/4; % Length of single airgap
A_air = (a1+l_gap/4)*(b+l_gap/4); % Gap area with fringing

% Iteration for the right number of turns
N_coil = 1; % Initial number of turns
L=1; % Inductance initial value

while L > 70e-6 || L < 60e-6
    N_coil = N_coil+0.5; % Number of turns
    R = l_gap/(y_0*A_air); % Reluctance of airgap
    L =N_coil^2/R; % Inductance
end

%Weight and loss calculation

c = wire_thickness*N_coil+20e-3; % Height of a leg
d = a1+2*a2+2*(wire_width+15e-3); % Width of the core
MPL_wire = 2*(a1+2*spacer)+2*(b+2*spacer); % Mean path length of wire
l_wire = MPL_wire*N_coil; % Total wire length
V_core = a1*b*c + 2*a2*b*c + 2*a2*b*d; % Volume of core
W_core = V_core*Fe_density*1000; % Weight of core
choke_length = c+2*a2; % Core total length
choke_width = d; % Core total width

```

```

B_new = L*I_RMS/(A_core*N_coil);           % Flux density

% If the dimensions of the design fit the inside the constraints
% resistance of the windings is calculated and the values are added to
% a matrix

if choke_width <= 202e-3 && choke_length <154e-3

[resistance, W_winding] = calculate_losses_DC(A_wire, l_wire, 0,
I_RMS);
W_total = W_core + W_winding;
data = [a1*1e3 a2*1e3 b*1e3 (c+2*a2)*1e3 d*1e3 wire_width*1e3 ...
        wire_thickness*1e3 resistance*1e3 W_winding/1000 W_core ...
        W_total B_new L*1e6 N_coil l_gap*1e3];
matrix(n,:) = data;
n = n + 1;

end
end
end
end
end

% Matrix is exported to filename.xlsx
filename = 'test_data.xlsx';
xlswrite(filename,matrix)

```